Industrial Crops & Products 246 (2026) 123417

Contents lists available at ScienceDirect

Industrial Crops & Products

journal homepage: www.elsevier.com/locate/indcrop

Biomass hard carbon for sodium-ion batteries: Feedstock-process-performance relationships

Yugen Bao [a], Tianyi Gao [a], Luxiang Ma [a,*], Yan Zhao [a], Hongli Su [b,*]

[a] College of Materials and Chemistry & Chemical Engineering, Chengdu University of Technology, Chengdu 610059, PR China
[b] Faculty of Civil Engineering and Geosciences, Delft University of Technology, Delft 2628 CN, the Netherlands

ARTICLE INFO

Keywords:
Agricultural residues
Sodium-ion battery
Biomass-derived hard carbon
Sodium storage mechanisms
Material modification

ABSTRACT

The conversion of agricultural residues into high-value-added biomass-derived hard carbon anodes for sodium-ion batteries not only achieves the valorization of agricultural resources but also shows considerable potential for addressing the global energy crisis and mitigating environmental pollution. However, the practical application of biomass-derived hard carbons is hindered by persistent challenges such as low specific capacity, low initial Coulombic efficiency, and poor cycling stability, stemming from an unclear structure-performance relationship between modification strategies and electrochemical behavior. This review summarizes established models describing sodium storage mechanisms in hard carbons, with particular emphasis on active storage sites such as nanopores, graphitic layers, and defect sites. Addressing the practical issues associated with biomass-derived hard carbons, several sodium storage mechanism models are discussed in detail, including the "insertion-filling", "adsorption-filling", "adsorption-insertion", and multistage mechanisms. Furthermore, relevant characterization analyses are integrated to elucidate the structure-performance relationship between hard carbon materials and sodium storage behavior. From a materials perspective, this review systematically outlines the preparation strategies, precursor selection, and the correlation between modification approaches and sodium storage mechanisms. Representative performance-enhancement strategies, including heteroatom doping, interfacial engineering, and morphology regulation, are explicitly summarized. Ultimately, in-depth investigation of these critical issues is expected to optimize the electrochemical performance of biomass-derived hard carbons and promote their practical application in sodium-ion batteries.

1. Introduction

Agricultural residues represent an abundant yet underutilized feedstock; their conversion into value-added carbon materials offers a direct route for waste reduction and advancing biomanufacturing (Fig. 1) (Table 1). Concurrently, the accelerating energy transition—enabled by the widespread deployment of electrochemical energy storage technologies—ensures a stable supply from intermittent sources and supports the energy demands of transportation and industry (Dhawale et al., 2023; Maka and Chaudhary, 2024; Su et al., 2024). This growing adoption, however, has placed considerable pressure on the sustainability and supply of battery materials, propelling sodium-ion batteries (SIBs) and carbon-based anodes to the forefront of research (Palomares et al., 2012; Wang et al., 2018a; Yang et al., 2021a, 2021b).

With escalating demand, the performance requirements for SIBs have become increasingly stringent. A SIB consists of a cathode, anode, electrolyte, and separator. Among these, the anode material is a critical component whose performance directly determines the full-cell electrochemical characteristics and largely dictates the system's economic viability. Therefore, developing high-performance SIB anodes has become a research priority. Current studies on sodium-storage anodes mainly focus on hard carbons, soft carbons (Jiang et al., 2021; Wang et al., 2018b), titanium-based compounds (Liang et al., 2018; Zhang et al., 2018), alloy-type materials (Liu et al., 2014; Qian et al., 2012), and metal compounds (Zhao et al., 2018, 2017). Among these, hard carbons stand out due to their low cost, structural diversity, good electrical conductivity, high sodium storage capacity, minimal volume change upon sodiation, environmental friendliness, and low redox potential (Alvin et al., 2021; Yabuuchi et al., 2014; Yan et al., 2021; Youn et al., 2021; Zhu et al., 2017). Based on precursors, hard carbons are classified into three types: biomass-derived, organic polymer-derived (Beda et al., 2018; Kamiyama et al., 2019; Zhang et al., 2021a, 2017),

* Corresponding authors.
E-mail addresses: maluxiang@cdut.edu.cn (L. Ma), h.su-3@tudelft.nl (H. Su).

https://doi.org/10.1016/j.indcrop.2026.123417
Received 19 March 2026; Received in revised form 17 April 2026; Accepted 4 May 2026
Available online 9 May 2026

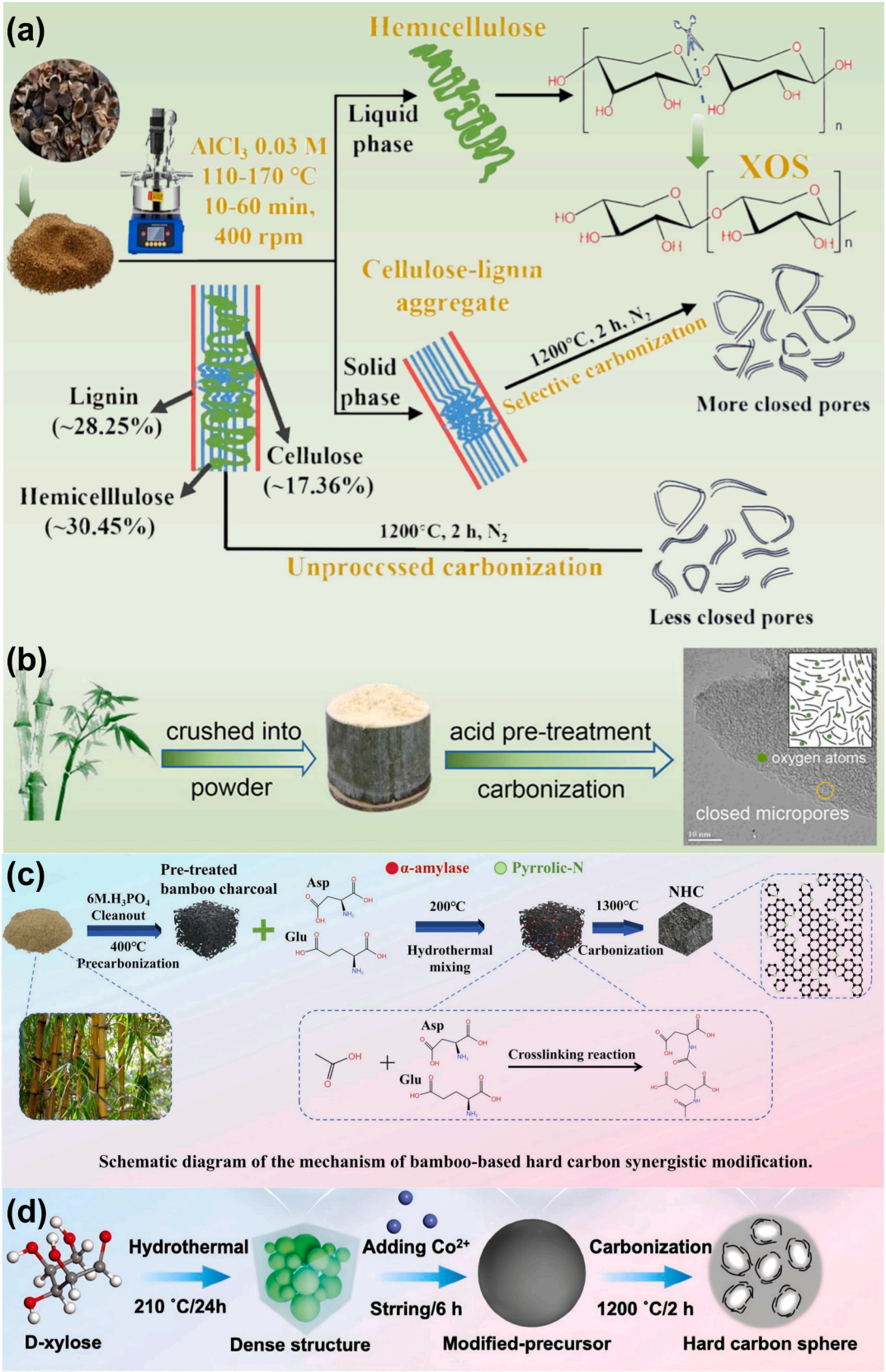

Fig. 1. Schematic illustration of representative processing routes for converting various biomass feedstocks (e.g., oil-tea camellia shells, bamboo, xylose) into hard carbon materials, including (a) catalytic hydrothermal pretreatment(Li et al., 2025a), (b) acid treatment modification(Xu et al., 2023b), (c) enzyme-assisted doping (Chen et al., 2026), and (d) hydrothermal coupled metal ion modification(Zhou et al., 2025).

and fossil fuel-derived (e.g., from coal, petroleum pitch, and coal tar pitch) (Daher et al., 2020; Li et al., 2016b; Lu et al., 2018). Biomass-derived hard carbons, prepared from agricultural and forestry wastes (e.g., straw, nutshells, pulp, and grains), have attracted considerable attention for SIB anodes due to their renewability, low cost, and eco-friendliness (Li et al., 2015; Lu et al., 2023a; Thompson et al., 2021; Wu et al., 2022b; Zheng et al., 2019). However, they face challenges related to ambiguous sodium storage mechanisms and an unclear structure–activity relationship between modification strategies and electrochemical performance (Gao, 2021; He et al., 2019; Kulova and Skundin, 2022; Lu et al., 2022; Xiao et al., 2018; Xie et al., 2019a; Yu et al., 2022a). These issues hinder performance enhancement. To overcome these limitations, it is essential to design, synthesize, and optimize hard carbon structures through in-depth investigation of the structure–activity relationship linking modification strategies and electrochemical outcomes.

Existing reviews largely compile preparation methods and electrochemical performance, lacking systematic analysis of this structure–activity relationship. In particular, the intrinsic links between precursor components and sodium storage mechanisms remain unexplored. To fill this gap, this review adopts a raw material–process–performance tripartite perspective. First, we critically compare the applicability conditions of four sodium storage mechanisms. Next, we correlate cellulose-rich, lignin-rich, and hemicellulose-rich precursors with closed-pore development, interlayer spacing, defect density, and plateau/slope capacity distribution. Then, we summarize the processing rules for heteroatom doping, interfacial engineering, and morphology regulation. Finally, we introduce a practical evaluation framework for full cells. This review aims to provide theoretical guidance for the rational design and performance optimization of biomass-derived hard carbon.

2. Sodium storage active sites in hard carbon

Although this review focuses on biomass-derived hard carbon, its sodium storage behavior fundamentally follows the general mechanisms of hard carbon materials. Accordingly, this section and Section 3 first systematically introduce the sodium storage active sites and mechanism models applicable to all hard carbons, laying a theoretical foundation for the subsequent discussion of biomass precursor characteristics and modification strategies.

Research has revealed that hard carbon typically comprises highly disordered graphene-like nanosheets, a high defect concentration, and abundant heteroatoms, resulting in structural heterogeneity and complexity (Xie et al., 2021). As an SIB anode material, its unique microstructure can be categorized from the perspective of Na^+ storage into nanopores, graphitic layers, and defect sites (Fig. 2), each exhibiting distinct Na^+ storage mechanisms. Therefore, understanding this complex structure is crucial for developing high-performance hard carbon anodes.

2.1. Nanopores for sodium storage

Nanopores are generally considered to store sodium ions via adsorption and filling mechanisms. According to the International Union of Pure and Applied Chemistry (IUPAC), these pores are classified into micropores (<2 nm), mesopores (2–50 nm), and macropores (>50 nm). In addition to conventional open pores in porous carbons, closed pores formed by folded and curved carbon layers are also widely accepted to exist within hard carbon materials. Open pores store sodium ions through surface adsorption, whereas closed pores store sodium ions via a filling mechanism. The controversies regarding the specific sodium storage mechanisms will be discussed below.

Stevens and Dahn (Stevens and Dahn, 2000a) first proposed the widely recognized "house-of-cards" model in 2000. This model posits that hard carbon is composed of numerous tiny, curved graphene nanosheets. These nanosheets stack in parallel to form graphitic microcrystallites with short-range order, which are then randomly arranged over long distances. Owing to the varying orientations of these graphitic microcrystallites, abundant nanopores are generated during this disordered stacking process. These nanopores are further categorized into open pores and closed pores (Fig. 3).

2.1.1. Adsorption mechanism in open-pore materials

Hard carbon materials typically feature abundant pore structures, which provide numerous active sites for sodium storage and facilitate ion migration and diffusion. Consequently, whether they are microporous carbons prepared by activation methods or mesoporous/macroporous carbons synthesized via template strategies, these materials generally exhibit high reversible capacity and excellent rate

Table 1
Summary table of the raw material–process–performance relationship for biomass-derived hard carbon anodes in sodium-ion batteries.

Precursor	Synthesis method	Modification method	Reversible capacity (mAh g^{-1})	ICE	Ref.
Waste wood	One-step heat treatment method	Regulated pore structure	350.7 mAh g^{-1} at 0.05 C	94.9%	(You et al., 2024)
Chitosan powder	Flash joule heating	Structural controls	187.9 mAh g^{-1} at 1 A g^{-1} after 2000 cycles		(Yuan et al., 2024b)
Natural bamboo	Deep eutectic solvent cell-shearing	Regulated pore structure	422 mAh g^{-1} at 30 mA g^{-1}	85.2%	(Lan et al., 2025)
	Van soest method	Regulated pore structure	350 mAh g^{-1} at 20 mA g^{-1}	90.3%	(Wang et al., 2024b)
Glucose	hydrothermal method	Pre-desolvation on the nanopore		98.21%	(Lu et al., 2024)
	MgO-template Synthesis	Regulated pore structure		88%	(Kamiyama et al., 2021)
Bamboo powder	Acid treatment in different steps	Adjusting the components of precursors	108.8 mAh g^{-1} at 8 A g^{-1}		(Wu et al., 2024a)
Sucrose	Temperature-controlled strategy	Balance graphitic nanodomains and heteroatom doping content	315 mAh g^{-1} at 0.2 A g^{-1}	98.82%	(Wang et al., 2024a)
Pinenut	One-step pyrolysis	Regulated pore structure	278 mAh g^{-1} at 0.2 A g^{-1}	85%	(Zhang et al., 2024c)
Cellulose	Temperature carbonized	Regulated structure			(Sun et al., 2020)
Bagasse	High-temperature thermal decomposition	Regulated structure		91.5%	(Hu et al., 2020)
Potassium-rich primitive gourd	Heating methods	Balances degree of graphitization and pore channel structure		90.7%	(LeGe et al., 2025)
Kapok fiber	Cross-linking carboxyl group in 2,6-pyridinedicarboxylic acid	N doping	401.7 mAh g^{-1} at 0.05 A g^{-1}		(Zhang et al., 2024b)
	Coulomb adsorption of methylene	N/S doping		99.44%	(Zhang et al., 2025c)
Bamboo fibers	High-temperature carbonization	Regulated pore structure	346 mAh g^{-1} at 50 A g^{-1}		(Huang et al., 2024)

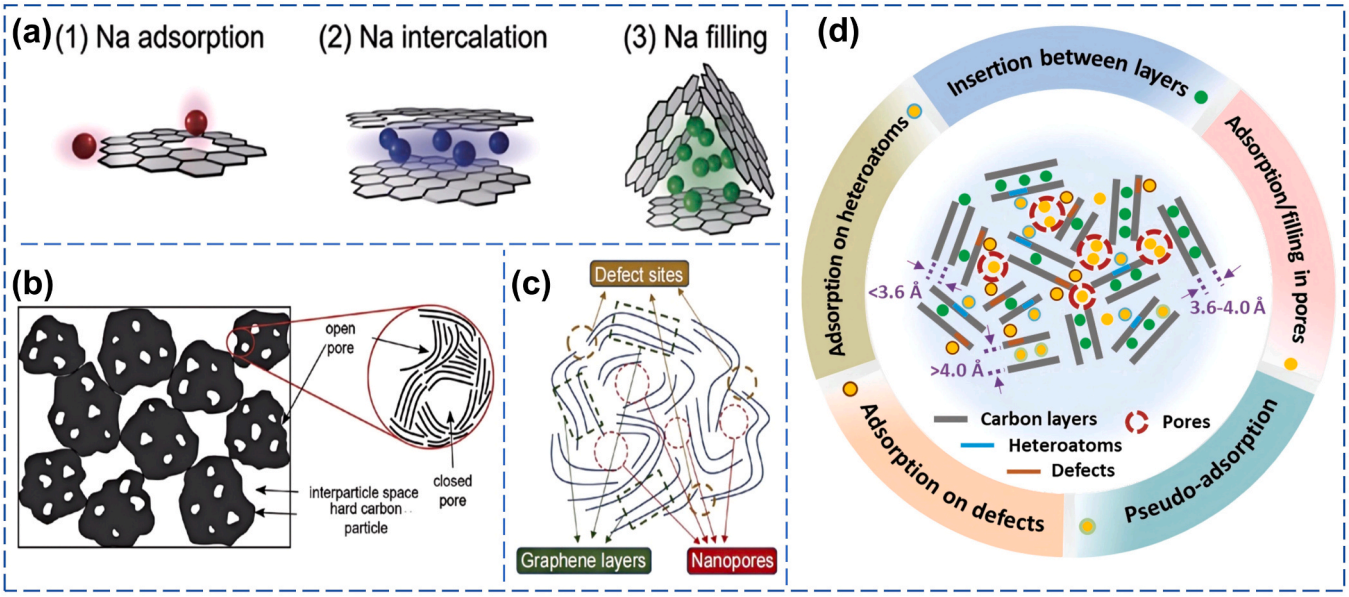

Fig. 2. Sodium storage active sites in hard carbon anode materials. (a) Microstructure of sodium storage sites(Morikawa et al., 2019); (b) Schematic illustration of open and closed pores in hard carbon(Kitsu Iglesias et al., 2023); (c) Sodium storage sites present in hard carbon(Cui et al., 2025b); (d) Schematic diagram of active sites for sodium storage in hard carbon and the possible corresponding sodium storage mechanisms(Sun et al., 2022).

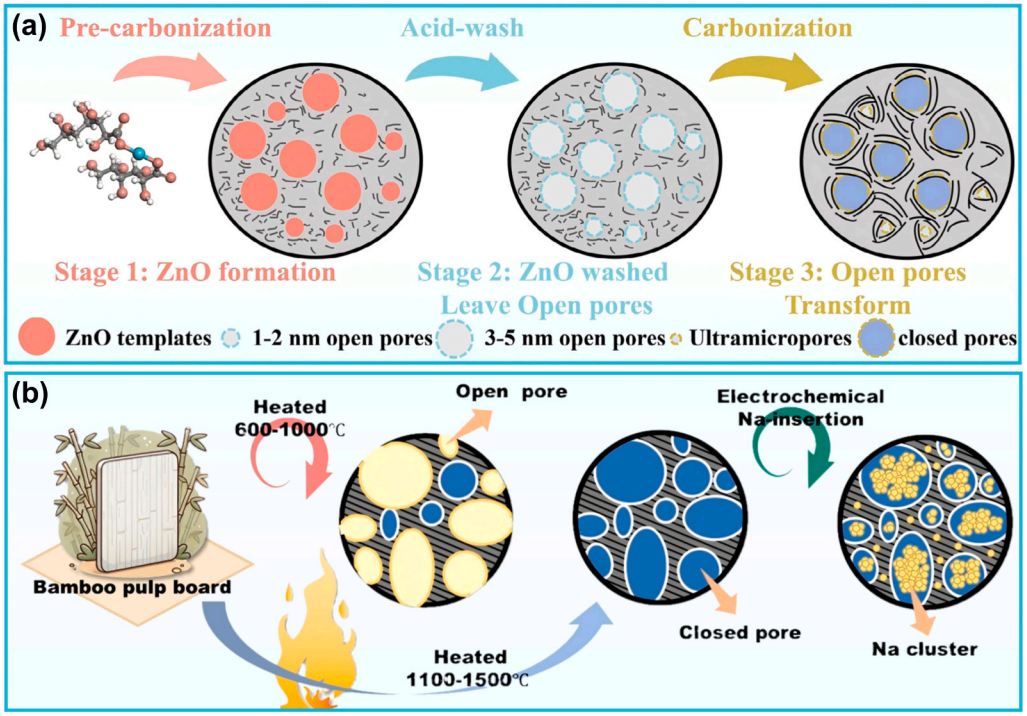

Fig. 3. Schematic illustration of the nanopore fabrication process in hard carbon materials. (a) Nanopore evolution mechanism in hard carbon materials synthesized via the ZnO template method(Ren et al., 2025); (b) Nanopore evolution mechanism in bamboo-derived biomass hard carbon materials(Sun et al., 2025c).

performance (Liu et al., 2016; Wenzel et al., 2011). However, due to their large specific surface area, the electrolyte decomposes on open pore surfaces during charge/discharge processes, forming a solid electrolyte interphase (SEI) film and causing irreversible Na^+ loss. As a result, these materials often show a low initial Coulombic efficiency (ICE) (Ren et al., 2025).

Gas (e.g., N_2, CO_2) adsorption/desorption remains the conventional method for characterizing the pore characteristics of carbon materials, with specific surface area (SBET) and pore volume (Vt) as two key parameters. However, due to the structural complexity of porous carbon materials, even carbons with identical SBET and Vt values can exhibit different porosity characteristics (Yang et al., 2020; Yu et al., 2018). Therefore, analyzing adsorption/desorption isotherms together with SBET and Vt values is necessary to obtain comprehensive porosity information. Additionally, scanning electron microscopy/high-resolution transmission electron microscopy (SEM/HRTEM) can be used for porosity analysis; porous carbons with low tap density typically exhibit loose morphologies and interconnected porosity (Yu et al., 2018).

SEM/HRTEM observations complement structural data from other characterization techniques, thereby validating conclusive structural analyses of hard carbon materials.

2.1.2. Filling mechanism in closed-pore materials

Closed pores are formed by folded and curved carbon layers. In contrast to the adsorption-controlled process occurring on open pore surfaces, the Na^+ storage process within closed pores is considered to be a diffusion-dominated mechanism(Au et al., 2020) (Fig. 4). As the pyrolysis temperature increases from 1000 to 1900 ℃, the low-voltage plateau capacity reaches a maximum at 1500 ℃ and then decreases. The authors attributed this phenomenon to the reduction in graphitic interlayer spacing, which diminishes the diffusion pathways available for Na^+ to enter the closed pores.

Among the characterization techniques for closed pores, small-angle X-ray scattering (SAXS) can detect closed pores within carbon materials and is therefore regarded as a powerful complementary technique to gas adsorption characterization(Saurel et al., 2018). By fitting the characteristic length scale to variations in scattering power between the medium and the pores, the radius of spherical closed pores can be inferred (Dou et al., 2019). SAXS analysis is sensitive to micropores and internal closed pores, enabling precise analysis of carbon structures. However, this technique is limited to the determination of average pore size, making it difficult to quantitatively analyze other important textural properties such as pore size distribution, pore volume, and surface area, which require specially designed and intensity-calibrated instruments. Consequently, true (skeletal) density measurement is widely employed to calculate the total volume of closed pores, complementing SAXS. Helium (He), as the analysis gas, can access almost all open pores except closed pores, allowing the true (skeletal) density value (ρ) to be determined using Archimedes' principle (Li et al., 2019b).

Currently, an in-depth understanding of the sodium storage process within nanopores is still in its infancy. The characterization of closed pores is crucial, yet it remains challenging to distinguish them from their open pore counterparts. A consensus on the sodium storage characteristics of open and closed pores has not yet been reached. Beyond developing advanced characterization techniques, this debate has also propelled the exploration of model carbon materials.

2.2. Graphitic layers for sodium storage

Graphite has a unique layered structure with an interlayer spacing of 0.335 nm, composed of stacked two-dimensional graphene sheets. However, the large ionic radius of Na^+ hinders its insertion between graphene layers to form intercalation compounds analogous to Li^+ (forming NaC_{64}) (Fig. 5a), resulting in a theoretical capacity of only 35 mAh g^{-1} (Luo et al., 2021; Wang et al., 2022; Zhang et al., 2021b; Zhao et al., 2020). Interlayer spacing and stacking misalignment are widely recognized as critical factors determining the feasibility of sodium storage between carbon layers (Fig. 5b). Cao et al. (Cao et al., 2012) simulated the energy cost of Na^+/Li^+ insertion into carbon as a function of interlayer distance. Their results indicate that the energy required for

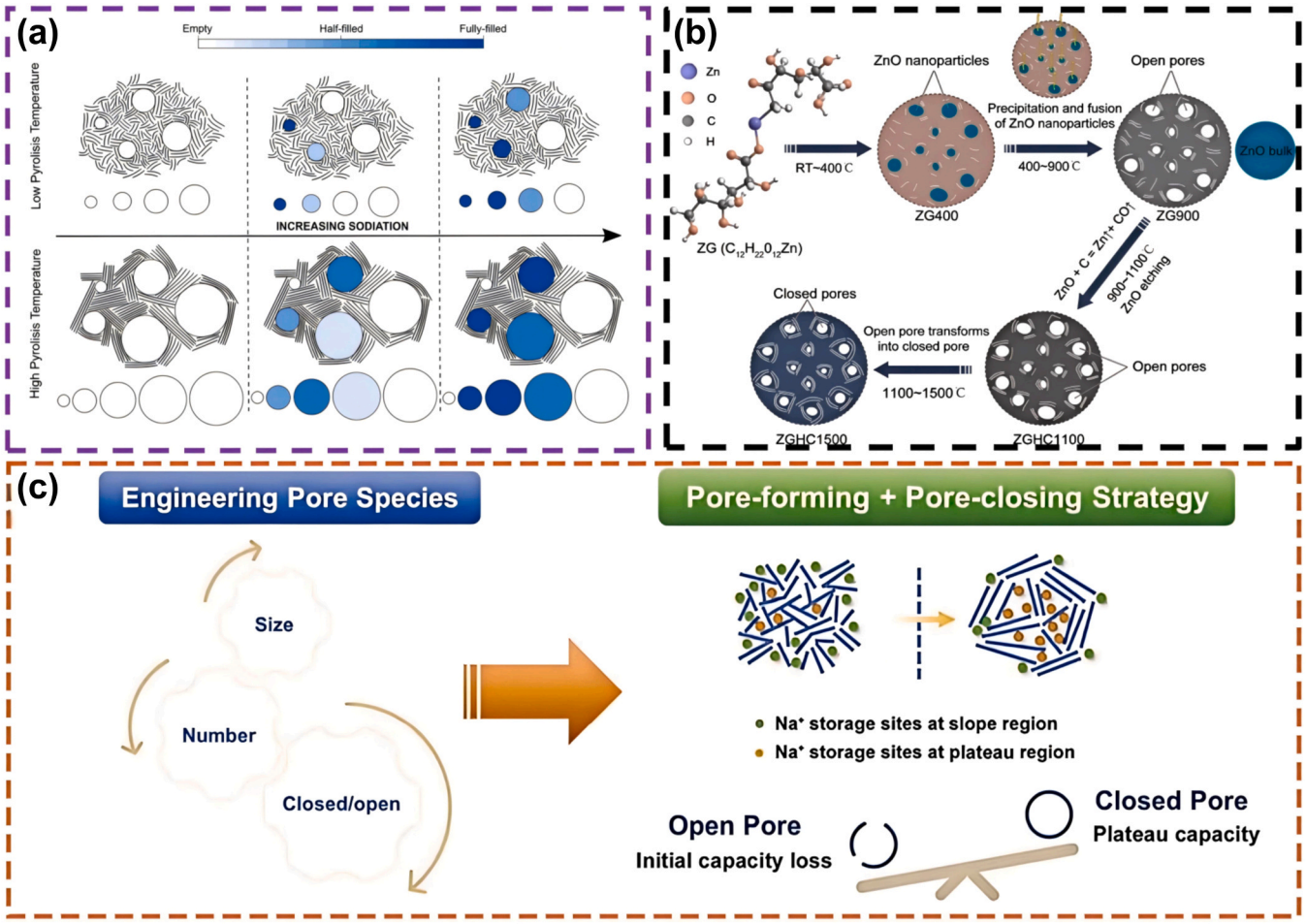

Fig. 4. Sodium storage mechanisms in closed/open pores and their regulation. (a) Schematic illustration of the microstructure of hard carbons synthesized at different pyrolysis temperatures and the corresponding sodium storage behavior within closed pores(Kitsu Iglesias et al., 2023); (b) Schematic diagram illustrating the closed pore formation mechanism during the pyrolysis of zinc gluconate(Qiu et al., 2024); (c) Schematic illustration of pore structure regulation in porous carbons (Li et al., 2019b).

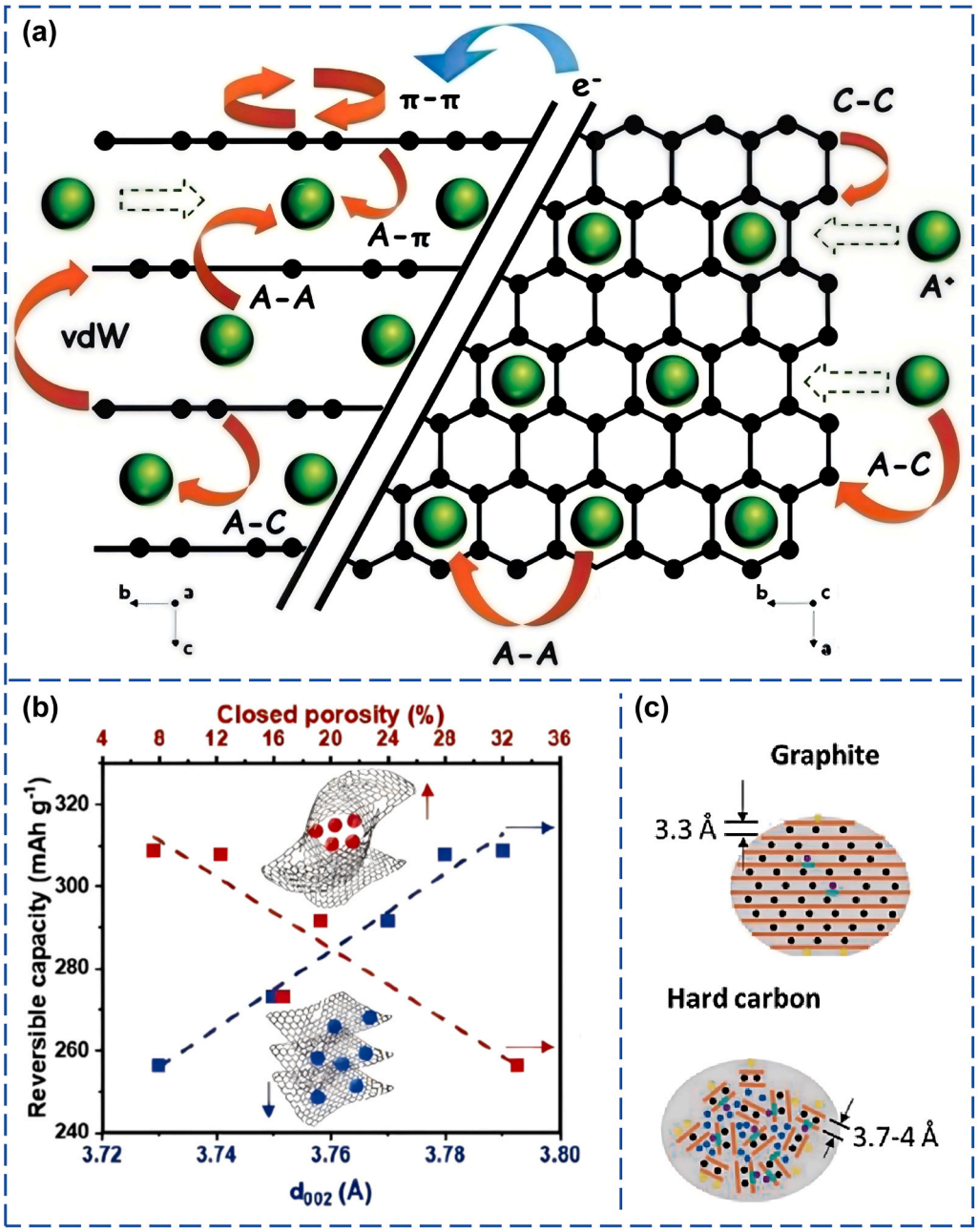

Fig. 5. Relationship between the structural characteristics of graphitic layer sodium storage sites and sodium storage performance. (a) Schematic diagram illustrating the bonding associated with the insertion of electropositive alkali metal ions into graphitic layers(Li et al., 2019a); (b) Correlation between reversible capacity and both closed porosity and the interlayer spacing (d_{002})(Escamilla-Pérez et al., 2023); (c) Structural differences between graphite and hard carbon(Xiao et al., 2019).

Na^+ insertion decreases with increasing interlayer spacing. When the spacing reaches 0.37 nm, the insertion energy barrier becomes sufficiently low, facilitating Na^+ intercalation. Notably, if the interlayer spacing of parallel graphene layers in hard carbon falls within 0.37–0.4 nm, Na^+ can form intercalation compounds similar to Li^+-graphite, exhibiting good sodium storage capability (Fig. 5c). When the spacing is below 0.36 nm, Na^+ insertion becomes highly difficult; above 0.4 nm, a pseudocapacitive effect emerges, and the storage mechanism shifts from intercalation to adsorption. Increasing the carbonization temperature, extending the holding time, and reducing the heating rate provide carbon atoms with sufficient energy and time for rearrangement, thereby enhancing the graphitization degree of hard carbon (Sun et al., 2019). Thus, the interlayer spacing can be controlled by modulating these carbonization parameters.

X-ray diffraction (XRD) is currently the most direct tool for analyzing the interlayer and microcrystalline structures of carbon materials. Carbons with different graphitization degrees and crystallinities yield distinctive XRD patterns (Tsai et al., 2015). Based on the interlayer spacing d_{002}, the carbon phase of hard carbon can be classified into three types (Sun et al., 2019): highly disordered phase ($d_{002} > 0.4$ nm), quasi-graphitic phase ($0.36\ \text{nm} < d_{002} < 0.40$ nm), and graphitic-like phase ($d_{002} < 0.36$ nm). High-resolution transmission electron microscopy (HRTEM) can be used for qualitative analysis of the crystal structure of hard carbon (Dou et al., 2019), while total neutron scattering coupled with pair distribution function (PDF) analysis is an advanced method for estimating crystalline domain or microcrystallite sizes. Due to the different physical principles underlying these techniques, calculated values generally show slight variations.

The graphitic microcrystalline structure (including interlayer spacing and microcrystallite size) is the most critical structural parameter determining the sodium storage performance of hard carbon. However, its characterization remains challenging. HRTEM can observe the degree of crystalline order but cannot provide quantitative information. XRD is the most commonly used method for analyzing interlayer spacing and microcrystalline structure, but the broad (002) diffraction peak of highly disordered hard carbon makes it difficult to accurately determine the peak position and estimate the interlayer spacing. The complex and heterogeneous microstructure of non-graphitic carbons, together with the coexistence of diverse microcrystalline regions, complicates the elucidation of the sodium storage mechanism. Furthermore, defect sites and nanopores also participate in sodium storage, adding further complexity. Therefore, more refined characterization techniques, fuller utilization of simulation methods, and the development of model hard carbons with uniform, controllable, and pore/defect-free microcrystalline structures will be essential for exploring the influence of microcrystalline structure on the sodium storage process.

2.3. Defect sites for sodium storage

Defects are intrinsic to hard carbon, including edge defects, vacancy defects, and heteroatom defects (Fig. 6a). Intrinsic defects (e.g., edge and vacancy defects) primarily modulate the local electronic structure, providing additional adsorption sites for Na^+ and contributing to high slope capacity. Moreover, their reversible adsorption/desorption behavior enables fast sodium storage kinetics, thereby enhancing rate performance (Li et al., 2018; Yuan et al., 2024a). In contrast, extrinsic defects (e.g., heteroatom doping with O, N, S, P) (Fig. 6b) introduce strong electronegative centers to increase Na^+ binding energy, expand the interlayer spacing, or induce additional intrinsic defects, synergistically improving reversible capacity and cycling stability (Ni et al., 2019; Zhang et al., 2023). Thus, the synergy between intrinsic and extrinsic defects is key to enhancing the overall electrochemical performance of hard carbon (Gan et al., 2025).

Raman spectroscopy is used to characterize structural irregularities and defect content in hard carbon (Dou et al., 2019; Ferrari, 2007; Ferrari and Basko, 2013). The Raman spectrum typically shows a D-band (defect band, ~1350 cm^{-1}) and a G-band (graphite band, ~1580 cm^{-1}). The D-band arises from vibrations of sp^2-hybridized carbon atoms in aromatic rings, while the G-band corresponds to bond stretching of all sp^2 atom pairs in both rings and chains. A 2D peak often appears at ~2700 cm^{-1}, indicating highly graphitized and ordered structures (Fig. 6c). The intensity ratio of the D-band to the G-band (ID/IG or ID/(ID+IG)) is commonly used to evaluate disorder degree and defect concentration. Furthermore, ratios among deconvoluted components (e.g., D1, D2, D3, D4, G) provide additional insights into the nature of structural defects.

Accurate defect analysis in hard carbon remains challenging due to the multitude of influencing factors. The complexity of structural defects and the difficulty in precisely determining their configurations further complicate the elucidation of charge storage mechanisms. Future research should enhance defect analysis accuracy through theoretical calculations, thereby establishing clearer correlations between defects and sodium storage mechanisms in hard carbon.

3. Sodium storage mechanism in HC

Understanding of the microstructure of hard carbon has evolved from Franklin's initial classification to the "house-of-cards" model and subsequently to fullerene-like structures (Ban et al., 1975; Franklin, 1951; Harris and Tsang, 1997; Stevens and Dahn, 2000a; Terzyk et al., 2007; Townsend et al., 1992). These early models laid the foundation for comprehending the complex structure of hard carbon, with the "house-of-cards" model directly prompting in-depth explorations of sodium storage mechanisms.

To date, the sodium storage mechanism of hard carbon remains controversial, with debate centered on the origin of capacity in the low-voltage plateau region (<0.1 V vs. Na^+/Na) and the high-voltage slope region (>0.1 V vs. Na^+/Na) (Chen et al., 2022; Ding et al., 2017; Kitsu Iglesias et al., 2023; Xue et al., 2025). Four main models have been proposed (Fig. 7): (1) the "insertion-filling" mechanism, (2) the "adsorption-filling" mechanism, (3) the "adsorption-insertion" mechanism, and (4) the multistage mechanism. Each model is supported by evidence, yet contradictions persist. This section systematically compares and critically evaluates them, aiming to determine under which conditions each mechanism dominates.

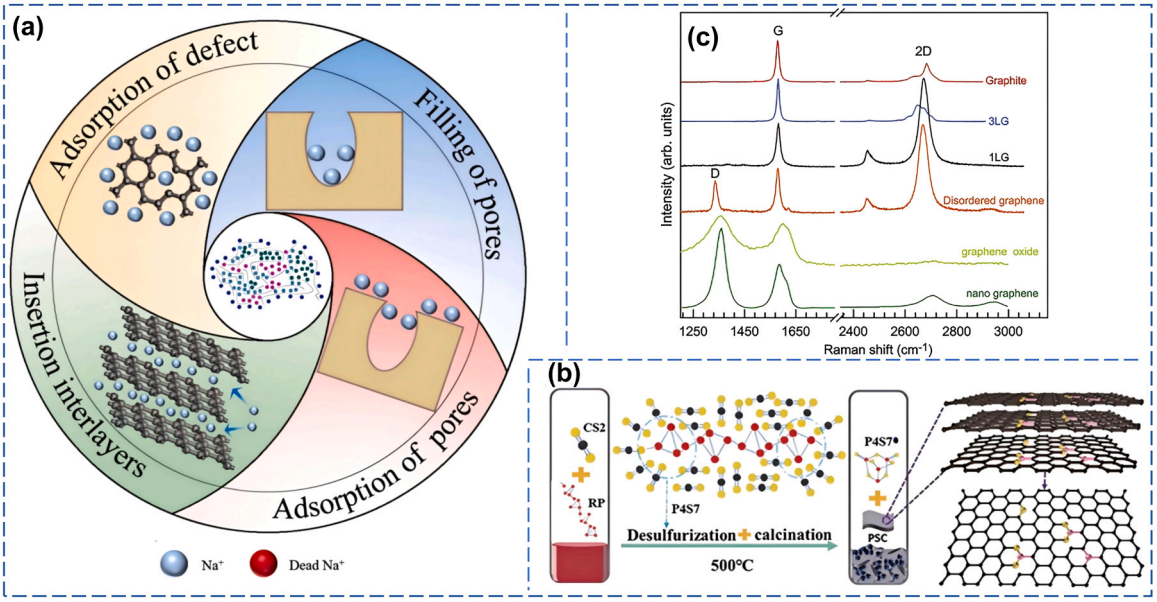

Fig. 6. Influence of defect sites on sodium storage mechanisms and their characterization. (a) Schematic illustration of the microstructure of hard carbon and the primary active centers responsible for Na^+ adsorption(Wang et al., 2025a); (b) Schematic diagram illustrating defects in phosphorus and sulfur co-doped carbon(Yan et al., 2020); (c) Raman spectra of graphene-based materials with different degrees of structural order(Wu et al., 2018b).

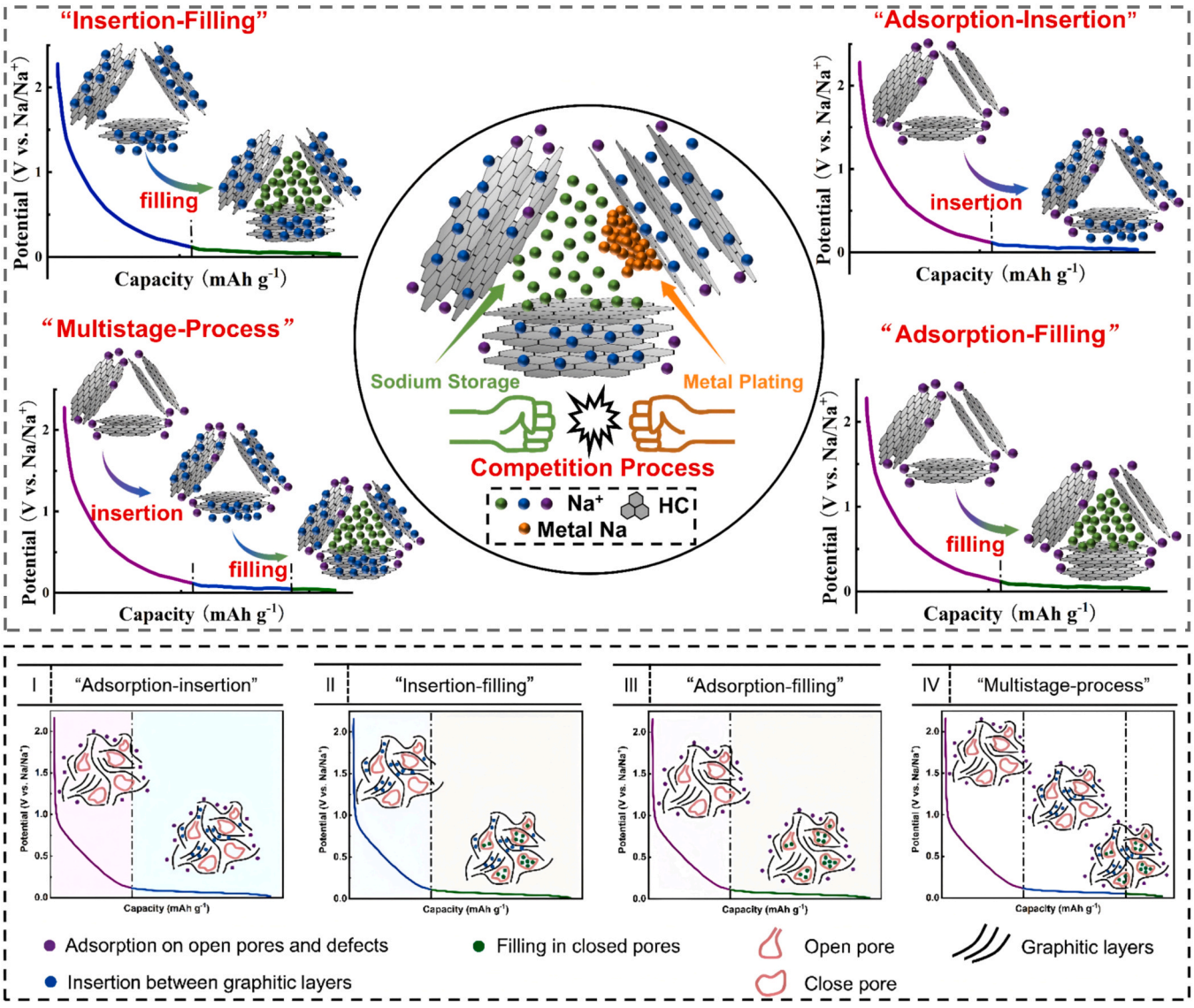

Fig. 7. Schematic diagram of sodium storage mechanism models for hard carbon(Zhou et al., 2024).

3.1. "Insertion-filling" mechanism

The core proposition of this mechanism is that slope region capacity arises from reversible Na^+ intercalation between graphitic-like layers, while plateau region capacity originates from Na^+ filling into open pores. Stevens and Dahn first proposed this model in 2000 (Stevens and Dahn, 2000a, b) based on in-situ SAXS and XRD studies of glucose-derived hard carbon. Evidence included a decrease in (002) peak intensity upon discharge and reduced nanopore scattering intensity in the low-voltage plateau region (Stevens and Dahn, 2001). Subsequently, Komaba et al. (Komaba et al., 2011) reproduced these phenomena in various hard carbons: ex-situ XRD showed gradual interlayer expansion from 2.0 V to 0.2 V; SAXS revealed a reversible decrease in scattering intensity at 0.03–0.07 $Å^{-1}$ in the plateau region; and Raman spectroscopy exhibited a red shift of the G-band in the slope region. These results were widely interpreted as direct evidence for intercalation (slope region) and open-pore filling (plateau region). Thereafter, similar trends were observed in nut shell-, cellulose-, and phenolic resin-derived hard carbons by Dahbi, Morita et al. (Dahbi et al., 2017), further consolidating this mechanism.

However, both core assumptions of this model have faced serious experimental challenges, fundamentally questioning its universality.

First, it attributes the entire slope capacity to intercalation. Yet many studies show that for defect-rich hard carbons (e.g., low-temperature pyrolyzed biomass), the slope capacity far exceeds the theoretical intercalation limit. For instance, in hard carbons rich in heteroatoms and edge defects, slope capacity can exceed 200 mAh g^{-1}, while pure intercalation typically contributes below 100 mAh g^{-1}. This discrepancy indicates that defect adsorption makes a non-negligible contribution to the slope region.

Second, it assumes that plateau capacity depends on open-pore filling. However, Li et al. (Li et al., 2016a) found a critical counterexample: as carbonization temperature increased from 1000 °C to 1600 °C, the open-pore specific surface area dropped from 538 m^2 g^{-1} to 14 m^2 g^{-1}, yet the plateau capacity increased significantly. If plateau capacity were solely due to open-pore filling, a decrease would be expected. This counterexample cannot be explained by the original "open-pore filling" model, but instead gave rise to the later "closed-pore filling" model.

Synthesizing the available evidence, we consider that the "insertion-filling" mechanism has strong explanatory power for carbon materials treated at high temperatures (>2000 °C), with few defects and structures approaching graphitization (e.g., high-temperature carbonized glucose- or pitch-derived carbons). Its advantages include direct support from in-situ SAXS and XRD evidence, as well as simplicity and

intuitiveness. However, for typical hard carbons (obtained by low-to-medium temperature pyrolysis, with high defect density and rich in closed pores), its applicability is limited—it underestimates defect adsorption's contribution to the slope region and fails to account for closed-pore-dominated plateau capacity. Consequently, subsequent studies have made important modifications to this model, either attributing the slope region to adsorption rather than intercalation, or ascribing the plateau region to closed-pore filling rather than open-pore filling.

3.2. "Adsorption-filling" mechanism

The core proposition of this mechanism contrasts with that of the "insertion-filling" mechanism: slope region capacity arises from Na^+ adsorption at defect sites and on graphene surfaces, while plateau region capacity originates from Na^+ filling into nanopores. However, two subversions must be distinguished: early studies attributed the plateau region to open-pore filling, but subsequent evidence pointed to closed-pore filling, which has become the mainstream view.

Zhang et al. (Zhang et al., 2015) found that as the carbonization temperature of PAN-derived CNF films increased to 2000 °C, the carbon interlayer spacing gradually decreased, while surface defects and heteroatoms significantly diminished. In-situ XRD showed no shift of the (002) peak, ruling out Na^+ intercalation. Under these conditions, the slope region almost completely disappeared, leaving only a single low-voltage plateau region. The authors therefore attributed the slope region to Na^+ adsorption on graphene surfaces or at defect sites, rather than to interlayer intercalation. Notably, the decrease in interlayer spacing and the disappearance of the slope region are concomitant phenomena of high-temperature carbonization; the former is not the direct cause of the latter.

To explain the critical counterexample of open-pore filling mentioned in Section 3.1, Li et al. (Li et al., 2016a) proposed a "closed-pore filling" model: plateau capacity originates from closed nanopores surrounded by parallel carbon layers, not from open pores (Fig. 8a). HRTEM showed that the number of closed pores increased after high-temperature carbonization, consistent with the increasing plateau capacity. Subsequently, Bai et al. (Bai et al., 2018) demonstrated through sulfur-filling experiments on micropores (Fig. 8b) that blocking micropores with sulfur eliminated the plateau capacity, indirectly supporting the pore-filling mechanism. More direct evidence came from operando SAXS by Kitsu Iglesias et al. (Kitsu Iglesias et al., 2023): in the plateau region, the scattering intensity of closed pores decreased significantly, indicating Na^+ entry into closed pores; in the slope region, the intensity changed only slightly, indicating that closed-pore filling occurs mainly in the plateau region (Fig. 8c).

Although the closed-pore filling model has become the mainstream explanation, several key issues remain unresolved: (i) Limitations of characterization techniques: HRTEM cannot clearly distinguish open from closed pores, and SAXS can only indirectly infer changes in closed-pore volume (Fig. 8d); atomic-scale techniques for directly observing sodium filling in closed pores are lacking. (ii) Lack of quantitative relationship: A reliable linear relationship between closed-pore volume and plateau capacity has not yet been established. In some studies, closed-pore volume increases while plateau capacity saturates, suggesting other limiting factors (e.g., pore entrance size, internal pore environment). (iii) Unclear processing rules for closed-pore formation: The relationships between closed-pore number/size and pyrolysis temperature/precursor type remain unsystematic, making "on-demand design" of closed-pore structures impossible.

3.3. "Adsorption-insertion" mechanism

The core proposition of this mechanism is that slope region capacity arises from Na^+ adsorption at defect sites and on graphene surfaces, while plateau region capacity originates from Na^+ intercalation between carbon layers. In contrast to the "adsorption-filling" mechanism, the

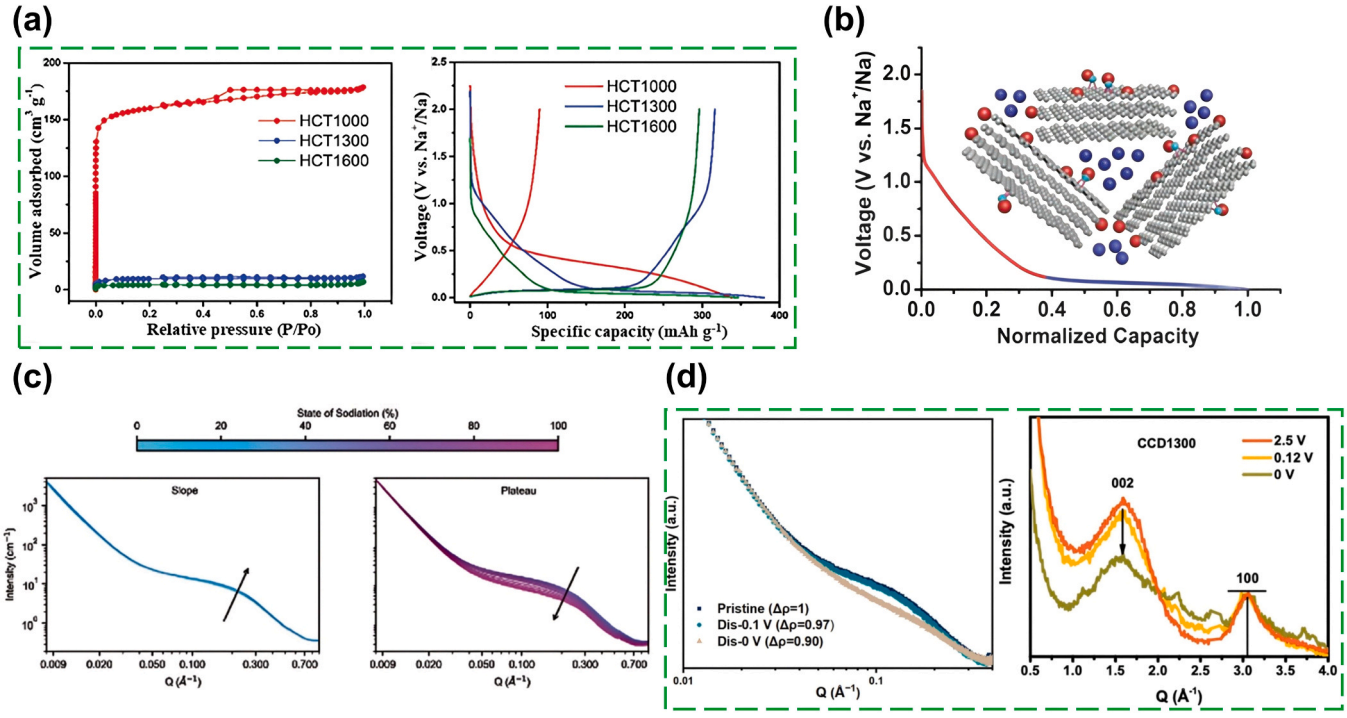

Fig. 8. Characterization of the relationship between closed pores and plateau capacity within the "adsorption-filling" mechanism. (a) Nitrogen adsorption-desorption isotherms depicting porosity evolution in hard carbon and the corresponding changes in plateau capacity for hard carbons prepared at different carbonization temperatures(Li et al., 2016a); (b) Schematic illustration of the sodium storage mechanism in hard carbon(Bai et al., 2018); (c) SAXS patterns of hard carbon in the slope capacity region and plateau capacity region(Kitsu Iglesias et al., 2023); (d) Ex-situ SAXS analysis and effective skeletal density measurements of carbon materials(Xie et al., 2019b).

plateau region is attributed to intercalation rather than pore filling.

Cao et al. (Cao et al., 2012) first proposed this model in 2012, finding that the CV curve of polyaniline-derived hollow carbon nanowires in the low-voltage region (0–0.2 V) closely resembled the intercalation peaks of Li^+ in graphite, suggesting that Na^+ also undergoes intercalation in the plateau region. Subsequently, Ding et al. (Ding et al., 2013) observed interlayer spacing expansion within the plateau region of peat moss-derived hard carbon using ex-situ XRD, supporting the intercalation hypothesis. More systematic evidence came from Bommier et al. (Bommier et al., 2015): they found a strong linear relationship between slope capacity and defect concentration (ID/IG), supporting an adsorption origin, while ex-situ XRD in the plateau region revealed reversible interlayer expansion/contraction, supporting intercalation. GITT measurements also showed a sharp drop in the diffusion coefficient in the plateau region (approximately 0.1–0.03 V), consistent with an intercalation process (Alvin et al., 2020). Sun et al. (Sun et al., 2019) further proposed an "extended adsorption-intercalation" model (Fig. 9), identifying the interlayer spacing d_{002} as the key parameter determining plateau capacity.

Although the "adsorption-insertion" mechanism is supported by substantial evidence, two anomalies severely challenge its core assumptions.

Anomaly 1: Low-temperature hard carbon exhibits a large interlayer spacing but lacks a plateau region. If the plateau region originated from intercalation, a larger spacing should favor intercalation and thus increase plateau capacity. However, in hard carbons prepared at low pyrolysis temperatures (<800 °C), even with interlayer spacing above 0.40 nm, the charge/discharge curves show almost no plateau region (only a slope region). This contradicts the intercalation model entirely.

Anomaly 2: Interlayer spacing decreases upon high-temperature carbonization, yet plateau capacity increases. As the pyrolysis temperature rises from 1000 °C to 1600 °C, d_{002} drops from ~0.40 nm to 0.38 nm or less. Intuitively, intercalation should become more difficult and plateau capacity should decrease. However, cotton-derived hard carbon (Li et al., 2016a) and phenolic resin-derived hard carbon (Jin et al., 2018) show that plateau capacity increases significantly as interlayer spacing decreases. This counterexample directly challenges the view that the plateau region mainly originates from intercalation.

These two anomalies together point to an alternative explanation: the plateau region likely arises primarily from closed-pore filling rather than intercalation. Closed pores develop more fully during high-temperature carbonization, consistent with the increasing plateau capacity; low-temperature hard carbon, despite its large interlayer spacing, has not yet formed closed pores, hence no plateau region.

The "adsorption-insertion" mechanism has the broadest explanatory scope among single-mechanism models. However, the above anomalies indicate that it significantly overestimates intercalation's contribution to the plateau region and underestimates that of closed-pore filling. In fact, the positive correlation between plateau capacity and closed-pore volume with increasing temperature is much stronger than its negative correlation with interlayer spacing. Therefore, we consider the pure "adsorption-insertion" model more suitable for specific hard carbons processed at medium carbonization temperatures (1000–1500 °C), with $d_{002} > 0.38$ nm and limited closed-pore development. For most typical hard carbons (especially biomass-derived, high-temperature carbonized samples), the plateau region is dominated by closed-pore filling, not intercalation. This is precisely why the multistage mechanism proposes that intercalation and filling jointly contribute to the plateau region.

3.4. *Multistage mechanism*

The three mechanisms introduced in the previous sections each emphasize different sodium storage processes, yet contradictions exist among them (Table 2). Recently, mounting evidence indicates that sodium storage in hard carbon is not a single process but rather the synergistic contribution of adsorption, intercalation, and filling across different voltage ranges and structural units, giving rise to the "multistage mechanism."

The most compelling evidence for the multistage mechanism comes from GITT measurements of the Na^+ diffusion coefficient as a function of voltage (Bommier et al., 2015; Jian et al., 2017; Li et al., 2017). Bommier et al. first reported that in glucose-derived hard carbon, the diffusion coefficient decreases slowly in the slope region (>0.1 V) (adsorption process), drops sharply in the initial plateau region (0.1–0.03 V) (intercalation process), and then unexpectedly rebounds at the end of the plateau region (<0.03 V) (closed-pore filling process). This three-stage variation has been reproduced in numerous subsequent studies (Alvira et al., 2023) (Fig. 10a).

Based on these findings, Jin et al. (Jin et al., 2018) proposed a "three-phase structure" model (Fig. 10b) and, according to the diffusion coefficient variation (Fig. 10c), subdivided the capacity into: (i) adsorption capacity (1.0–0.1 V): from Na^+ adsorption at defect sites,

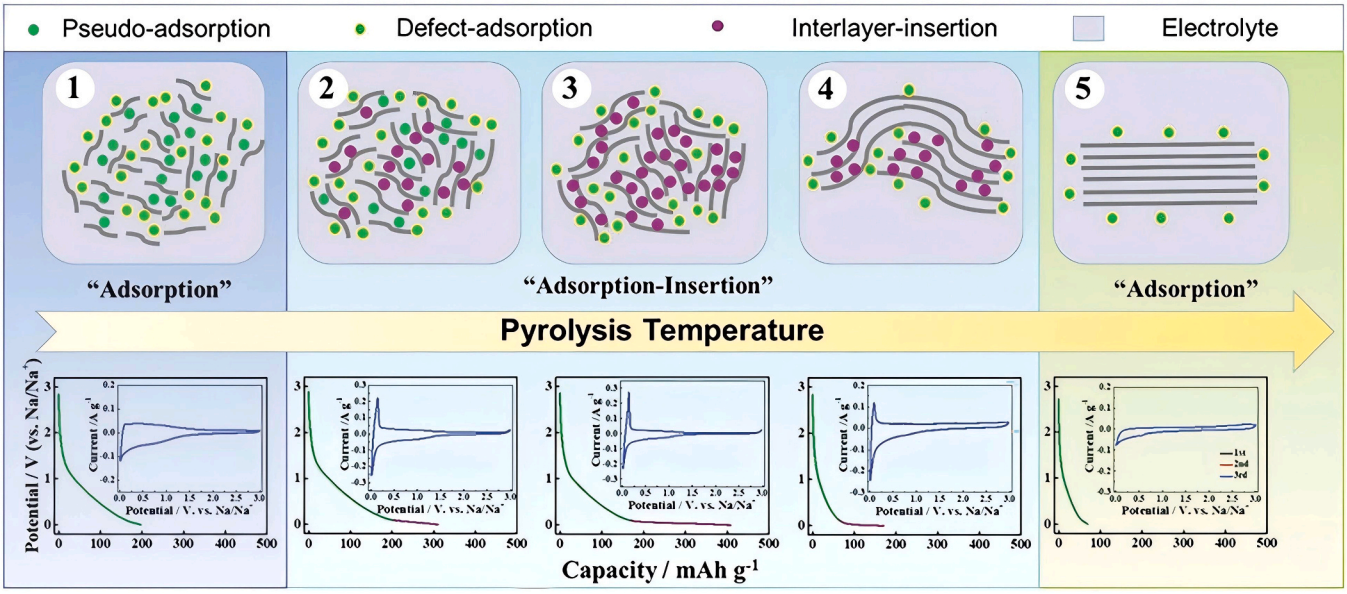

Fig. 9. Extended model of the "adsorption-insertion" sodium storage mechanism(Sun et al., 2019).

Table 2
Summary comparison of the four sodium storage mechanisms.

Sodium storage mechanism	Origin of slope region	Origin of plateau region	Key experimental evidence	Limitations	Characteristics of applicable carbon materials (pyrolysis temperature / precursor)	Ref.
Insertion-filling	Intercalation	Open-pore filling	In-situ SAXS (decreased scattering intensity in plateau region); in-situ XRD ((002) peak shift)	Ignores contribution of defects to slope region; cannot explain counterexample of decreased open pores but increased plateau capacity	High-temperature carbonization (>2000 ℃) / graphitizable precursors (pitch, aromatic polymers)	(Komaba et al., 2011; Stevens and Dahn, 2000a, 2001)
Adsorption-filling	Adsorption	Closed-pore filling	Operando SAXS (decreased closed-pore scattering in plateau region); sulfur filling experiments (disappearance of plateau)	Lack of direct characterization techniques for closed pores; no bidirectional linear relationship between closed-pore volume and plateau capacity	Medium-temperature carbonization (800–1200 ℃) / biomass or heteroatom-containing polymers	(Bai et al., 2018; Kitsu Iglesias et al., 2023; Li et al., 2016a)
Adsorption-insertion	Adsorption	Intercalation	GITT (decreased diffusion coefficient in plateau region); ex-situ XRD (reversible interlayer expansion)	Cannot explain absence of plateau in low-temperature hard carbon (large interlayer spacing) nor increased plateau in high-temperature hard carbon (decreased interlayer spacing)	Medium-temperature carbonization (1000–1500 ℃) / precursors with interlayer spacing d_{002} > 0.38 nm and few closed pores	(Alvin et al., 2020; Bommier et al., 2015; Cao et al., 2012)
Multistage	Adsorption	Intercalation and closed-pore filling	GITT three-stage diffusion coefficient (slow, then sharp drop, then rebound); combined SAXS and NMR	Unclear state of sodium in final stage (metallic/quasi-metallic/ ionic); difficulty in quantitative decoupling of intercalation and filling contributions	Wide temperature range (800–1600 ℃) / various precursors (especially suitable for biomass and resins)	(Jin et al., 2018; Kitsu Iglesias et al., 2023; Vasileiadis et al., 2023)

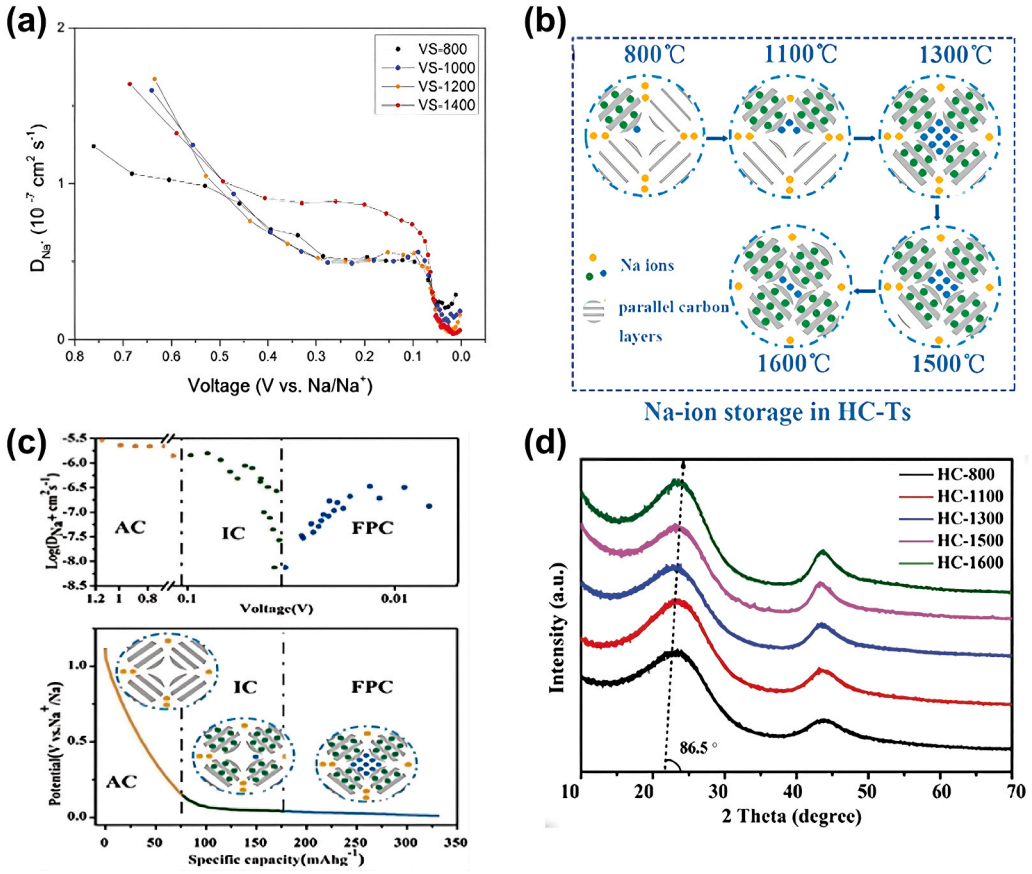

Fig. 10. X-ray diffraction and other characterizations of the "multistage mechanism." (a) DNa^+ values calculated from GITT measurements during sodiation(Alvira et al., 2023); (b) Adsorption/intercalation/filling contributions in hard carbon at different carbonization temperatures(Jin et al., 2018); (c) Variation of sodium ion diffusion coefficient in hard carbon electrodes with voltage and the corresponding sodium storage mechanisms(Jin et al., 2018); (d) X-ray diffraction patterns of hard carbon carbonized at different temperatures(Jin et al., 2018).

edges, and surfaces; (ii) intercalation capacity (0.1–0.03 V): from Na^+ insertion between graphitic-like layers; (iii) filling capacity (0.03–0 V): from Na^+ closed-pore filling. By processing the crosslinking degree of phenolic resin and the carbonization temperature (Fig. 10d), they found that with increasing temperature, adsorption capacity gradually decreased (due to defect reduction), intercalation capacity first

increased and then decreased (as interlayer spacing first increased then decreased), and filling capacity continuously increased (due to closed-pore development). The superposition of these three contributions successfully explained the non-monotonic trend of plateau capacity with temperature. Furthermore, in-situ XRD, ex-situ Raman spectroscopy, SAXS analysis, and DFT calculations (Kitsu Iglesias et al., 2023) have confirmed this mechanism.

Synthesizing the available evidence, we consider the multistage mechanism to be the model that most closely approximates the actual sodium storage process under current knowledge, for the following reasons: (i) Strongest explanatory power: it simultaneously accounts for multiple cross-scale phenomena, including the absence of a plateau region in low-temperature hard carbon, the decrease in interlayer spacing but increase in plateau capacity in high-temperature hard carbon, the three-stage variation of the GITT diffusion coefficient, and the changes in SAXS closed-pore scattering. (ii) Complete chain of evidence: it has been cross-validated by independent techniques including GITT, in-situ XRD, SAXS, Raman spectroscopy, NMR, and DFT calculations. (iii) Unification of controversies: it incorporates three seemingly opposing models—"insertion-filling," "adsorption-filling," and "adsorption-insertion"—as special cases within a general framework. When closed pores are absent, the multistage mechanism degenerates into adsorption-insertion; when intercalation contribution is negligible, it degenerates into adsorption-filling; and when open-pore filling is considered, it partially approaches insertion-filling.

As shown in Table 2, biomass-derived hard carbon does not possess a fundamentally different sodium storage mechanism from other hard carbons (e.g., polymer-based or fossil-based); the sodium storage behavior of all hard carbons can be uniformly described by the four mechanisms presented in this section, especially the multistage mechanism. The fundamental differences lie not at the mechanistic level but at the structural level: the unique cellulose/lignin/hemicellulose ratios, natural nanostructures, and heteroatom contents of biomass precursors affect the degree of closed-pore development, defect density, and graphitic interlayer spacing and orientation, thereby altering the relative proportions of adsorption, intercalation, and closed-pore filling contributions, manifested as different distributions of plateau/slope capacity.

After nearly two decades of debate, the four sodium storage mechanisms have evolved from being "mutually exclusive" to "complementary." The multistage mechanism, as a unifying framework, is supported by the majority of current evidence. However, its core bottleneck—the inability to quantitatively decouple the contributions of intercalation and filling—still constrains the transition from "mechanism description" to "material design." Future breakthroughs may come from the following directions: (i) In-situ cryo-electron microscopy: directly observing the atomic arrangement of sodium within closed pores to clarify its metallic/quasi-metallic/ionic state. (ii) Combined operando techniques: simultaneously acquiring SAXS (to monitor closed-pore filling) and XRD (to monitor intercalation), coupled with machine learning to decouple the two contributions. (iii) Model hard carbon systems: designing model materials with a single variable, such as varying only closed-pore volume or only interlayer spacing, thereby systematically verifying the quantitative relationships of each mechanism.

We anticipate that the comparative framework provided in this review will help researchers rapidly identify the most appropriate sodium storage mechanism for their specific material systems and offer theoretical guidance for the rational design of high-performance biomass-derived hard carbon anodes.

4. Structure-activity relationship between hard carbon precursor characteristics and sodium storage strategies

Hard carbon materials possess abundant interwoven and stacked graphitic microcrystallite layers, micropores, and defects, with these microstructural features primarily determined by their precursors. Owing to variations in the initial microstructures of different biomass sources, biomass-derived hard carbons from distinct precursors exhibit different electrochemical performances. Cellulose mainly contributes to plateau capacity; untreated lignin primarily contributes to slope capacity, whereas purified lignin after washing optimization predominantly contributes to plateau capacity. Additionally, the removal of hemicellulose can also enhance plateau capacity (Fig. 11).

4.1. Cellulose-rich biomass-derived hard carbon materials

For cellulose-rich biomass-derived hard carbon materials, high-temperature carbonization (>1000 °C) drives the cellulose-derived graphitic-like layers to undergo curling, folding, and cross-linking. Owing to the oxygen-rich nature of cellulose precursors, cross-linked structures readily form, promoting the formation of closed pores at high temperatures rather than fully graphitized structures (Cui et al., 2025a) (Fig. 12a). Moreover, cellulose-based materials consist of microfibers assembled via hydrogen bonds and van der Waals forces; upon carbonization, this architecture provides a spatial pore structure. Huang et al. (Huang et al., 2024) proposed a "deconstruction engineering" strategy, in which the disordered lignin and hemicellulose components in bamboo fibers were selectively etched away with NaOH, thereby enriching the cellulose content (Fig. 12g). Untreated lignin-rich precursors tend to form disordered carbon structures, whereas the abundant oxygen-containing functional groups in cellulose-rich precursors induce strong cross-linking, bending, and folding of carbon layers during pyrolysis, ultimately forming curved/coiled "pseudo-graphitic domains." These curved pseudo-graphitic sheets interconnect to form the "pore walls" of closed pores, effectively promoting closed-pore formation and increasing the plateau capacity by approximately 53% (from 166 to 254 mAh g^{-1}), confirming cellulose as a key component for constructing hard carbon with high closed-pore volume. Consequently, its sodium storage behavior mainly manifests as a closed-pore filling process in the low-voltage plateau region.

4.2. Lignin-rich biomass-derived hard carbon materials

For lignin-rich biomass-derived hard carbon materials, untreated lignin-derived carbon contains abundant impurities, surface defects, and a high specific surface area, providing numerous adsorption sites and thus a high slope capacity. Removing impurities and reducing the specific surface area via water washing decreases surface adsorption sites, lowering the proportion of slope capacity. Simultaneously, the internal graphitic-like structures and closed pores become more favorable for sodium insertion and filling, thereby significantly enhancing plateau capacity (Dayarathne et al., 2025; Matei Ghimbeu et al., 2019) (Fig. 12b-d). Sun et al. (Sun et al., 2025b) investigated industrial hardwood lignin and found that after treatment at 1500 °C, it tends to form short-range ordered turbostratic graphitic domains and a high concentration of closed nanopores (Fig. 12e,f). Based on these findings, the authors proposed an "adsorption-insertion-filling" mechanism: benefiting from the closed-pore structure derived from precursor transformation, the optimized hard carbon exhibits exceptional Na^+ filling behavior in the low-potential plateau region (<0.1 V), achieving synergistic enhancement of reversible capacity (338 mAh g^{-1}) and initial Coulombic efficiency (87%).

Compared with cellulose-rich biomass-derived hard carbon, lignin-rich hard carbon, owing to its aromatic-ring-rich precursor, tends to form relatively straight but highly disordered layer-stacked "turbostratic graphitic domains" during pyrolysis. Such structures possess a wider interlayer spacing (typically > 0.37 nm) and abundant edge defects, providing rapid intercalation and adsorption sites for Na^+. Consequently, its sodium storage behavior is more focused on adsorption and intercalation in the high-voltage slope region, typically exhibiting high slope capacity and excellent rate performance. In brief, cellulose-derived "pseudo-graphitic" structures emphasize closed-pore formation,

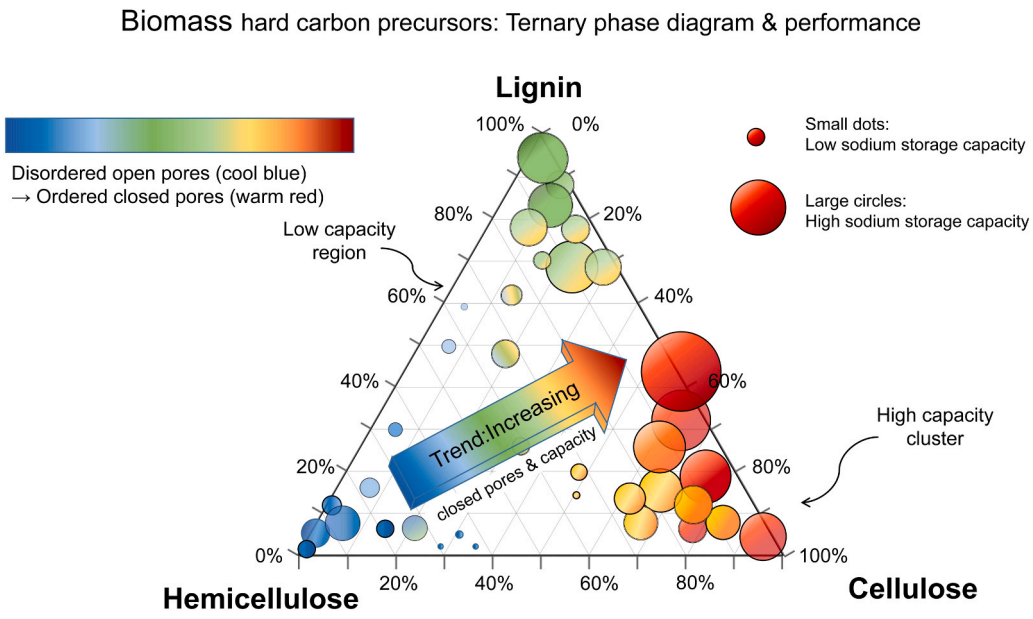

Fig. 11. Schematic diagram illustrating the structure-activity relationship between the compositional characteristics of biomass-derived hard carbon precursors and their sodium storage performance.

whereas lignin-derived "turbostratic graphitic" structures emphasize interlayer spacing expansion and provision of adsorption sites. Understanding this microstructural difference is fundamental for precisely processing the plateau/slope capacity and electrochemical behavior of biomass-derived hard carbon.

4.3. Hemicellulose-rich biomass-derived hard carbon materials

In contrast to cellulose-rich and lignin-rich biomass-derived hard carbons, hemicellulose-rich counterparts often exhibit low initial Coulombic efficiency and poor cycling performance (Dou et al., 2017). Owing to its poor thermal stability, hemicellulose preferentially decomposes and carbonizes during the low-temperature stage (200–400 °C), forming oxygen-lean, ordered carbon structures that act as "barriers, " blocking cross-linking reactions between cellulose- and lignin-derived oxygen-rich carbon domains. Lacking cross-linking constraints, the carbon layers readily rearrange and slide at high temperatures, ultimately forming long-range ordered graphite-like structures with narrow interlayer spacing and minimal closed porosity—both unfavorable for sodium storage. Fu et al. (Fu et al., 2025) proposed a structural regulation strategy based on hemicellulose removal, noting that hemicellulose hinders the formation of C(O)O cross-linking bonds at high temperatures, which are critical for inducing closed pores. After hemicellulose removal by alkali treatment, the precursor retained more oxygen-containing functional groups during the 400–600 °C stage and formed a stable cross-linked network. Subsequent high-temperature decomposition (600–700 °C) generated pores in situ, which ultimately evolved into closed pores. SAXS and true density measurements confirmed that the optimized sample (TC-10%) possessed the largest closed-pore volume, corresponding to significantly enhanced plateau capacity (174 mAh g^{-1}) and excellent initial Coulombic efficiency (80.5%) (Fig. 12h).

Therefore, based on the microstructure of hard carbon, the rational selection and processing of precursors constitute a key strategy for enhancing the sodium storage performance and overall electrochemical properties of hard carbon materials. The intrinsic relationship between these microstructural characteristics and the sodium storage mechanisms underpins the understanding of the sodium storage behavior in hard carbon and serves as the foundation for material modification.

5. Heteroatom doping

Heteroatom doping significantly influences the sodium storage performance of hard carbon materials. Introducing heteroatoms creates additional defects and active sites, enhances electronic conductivity, strengthens Na^+ adsorption, induces more defects, and moderately expands the interlayer spacing of graphitic microcrystallites, thereby effectively improving electrochemical performance.

However, current research mainly consists of case reports on single-element doping, lacking cross-comparisons and systematic summaries of the mechanisms of different dopant elements. This section first condenses the core parameters and effects of representative N, P, and S doping studies in a summary table (Table 3), then provides a categorized review of the unique mechanisms, key contradictions, and synergistic rules for each element, aiming to rationalize the selection of doping strategies.

5.1. N doping

Nitrogen doping is the most widely adopted strategy for modifying hard carbon, and its benefits for sodium storage mainly arise from two mechanisms. First, pyridinic N and pyrrolic N, as the primary active configurations, introduce abundant defect sites by inducing local distortion of the carbon skeleton, significantly enhancing Na^+ adsorption capacity in the slope region (Patel et al., 2024) (Fig. 13a). Second, the incorporation of N atoms moderately expands the interlayer spacing of graphitic microcrystallites, reducing the diffusion energy barrier for Na^+ intercalation (Agrawal et al., 2019). However, recent studies show that the specific effect of N doping highly depends on the synergistic processing of doping timing and nitrogen configuration.

Based on this understanding, Zhang et al. (Zhang et al., 2024b) proposed a "pre-crosslinking-assisted pyrolysis" strategy (one-step method): introducing a nitrogen-containing crosslinker before carbonization allows nitrogen atoms to participate in carbon skeleton construction at the early pyrolysis stage (Fig. 13b, c). This pathway is dominated by defect generation; the high proportion of pyridinic/pyrrolic nitrogen effectively enhances slope adsorption capacity, albeit with limited contribution to the plateau region. To address the long-standing challenge of balancing high graphitization degree with abundant active sites, Huang et al. (Huang et al., 2025) proposed a

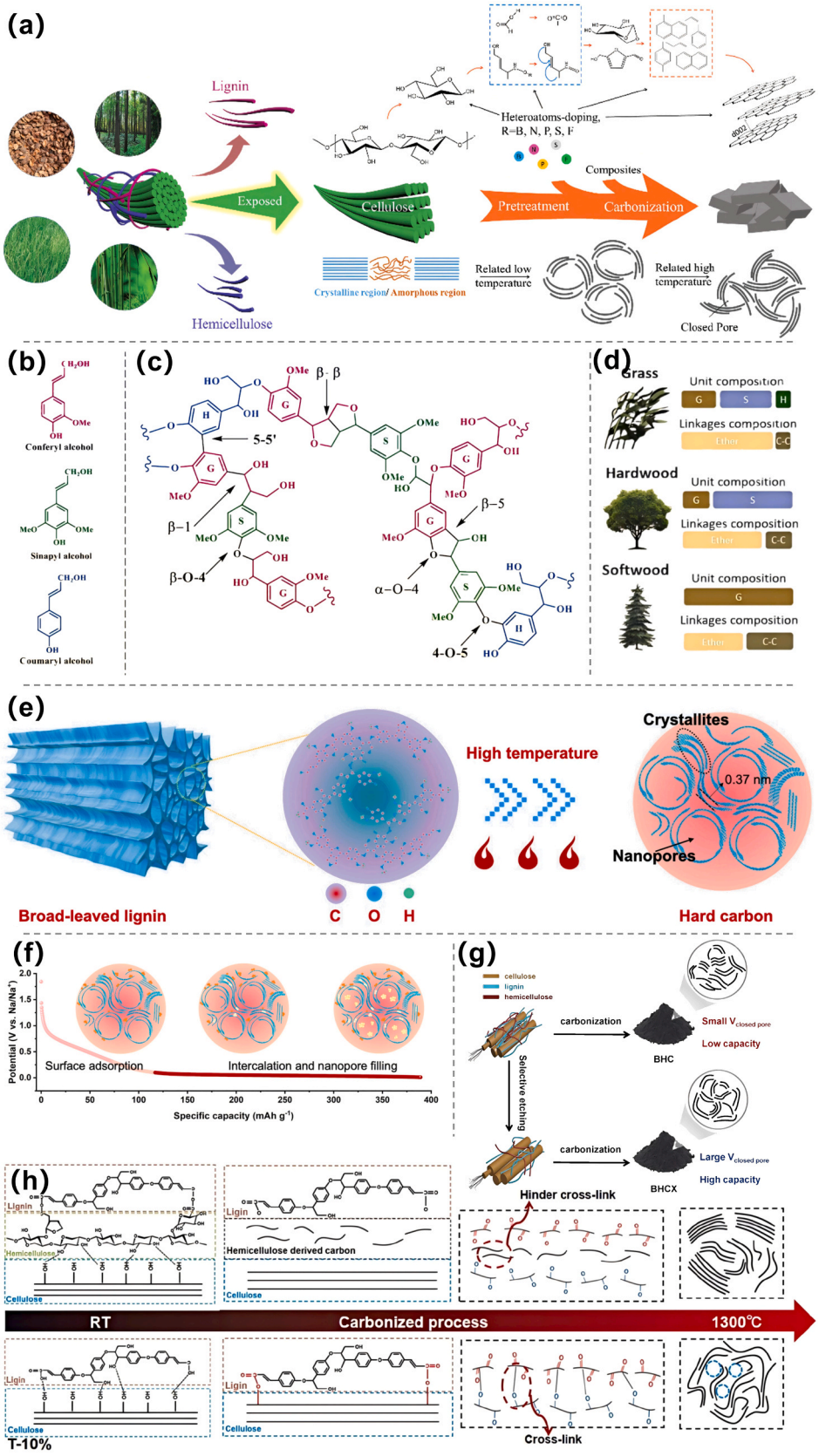

Fig. 12. Preparation of hard carbon from precursors with varying cellulose/lignin/hemicellulose ratios and the corresponding sodium storage mechanisms. (a) Schematic illustration of the fabrication process and microstructural evolution of bamboo fiber-derived hard carbon(Cui et al#, 2025a); (b-d) Chemical structures of lignin monomers from different sources and the typical inter-unit linkages(Dayarathne et al#, 2025); (e-f) Schematic diagram of the preparation process for lignin-derived hard carbon and its sodium storage mechanism(Sun et al#, 2025b); (g) Preparation process of bamboo-based hard carbon(Huang et al#, 2024); (h) Schematic illustration of the processing mechanism of hemicellulose removal on closed pore formation(Fu et al#, 2025).

Table 3
Summary of representative heteroatom doping strategies, structural effects, and electrochemical performance in hard carbon materials.

Doping Element	Precursor / Strategy	Key Structural Modifications	Electrochemical Highlights	Ref.
N	2,6-Pyridinedicarboxylic acid, pre-crosslinking-assisted pyrolysis	Increased pyridinic/pyrrolic N, d_{002} = 0.387 nm, increased defect sites	High slope capacity: 401.7 mAh g^{-1} at 0.05 A g^{-1}	(Zhang et al., 2024b)
	Melamine post-treatment, 1300 °C carbon skeleton	d_{002} = 0.393 nm, increased closed pores, Na_3N-rich SEI film	High plateau capacity and ICE: 350.1 mAh g^{-1}, ICE 90.1%	(Huang et al., 2025)
P	the oxygen-free liquid-phase precursor bubbling method	30 wt% P, P–(C_3) protrusion structure, d_{002} = 0.385 nm, metallic-like conductivity	Ultra-high rate: 397.1 mAh g^{-1} at 10 A g^{-1}	(Yan et al., 2021)
	Solution plasma treatment of triphenylphosphine	4 P, increased topological defects, surface-capacitance dominated	Extremely long cycle life: 83 mAh g^{-1} after 40,000 cycles at 100 A g^{-1}	(Kim et al., 2020)
S	In-situ gas-phase etching with sulfur vapor	89.9% thiophenic S, interconnected microporous network	Excellent rate performance: 373.5 mAh g^{-1} at 7 A g^{-1}	(Sun et al., 2025a)
	CVD surface sulfurization	C–S–C surface bonding, Na^+ adsorption energy tuned from −1.39 eV to −1.15 eV	ICE enhancement: from 52% to 73%	(de Tomas et al., 2023)
N/P	Interfacial polymerization	Low specific surface area, synergistic interlayer expansion and defects	144 mAh g^{-1} at 10 A g^{-1}	(Wu et al., 2022a, 2024b)
N/O	Ammonia modification of Xanthium sibiricum	Increased pyridinic/pyrrolic N and C═O functional groups	96.8% capacity retention after 2000 cycles	(Zhang et al., 2019)
N/S	KNO_3 combustion activation and N-allylthiourea treatment	2D porous carbon sheets, high specific surface area	143.1 mAh g^{-1} at 5 A g^{-1}	(Zhang et al., 2024a)

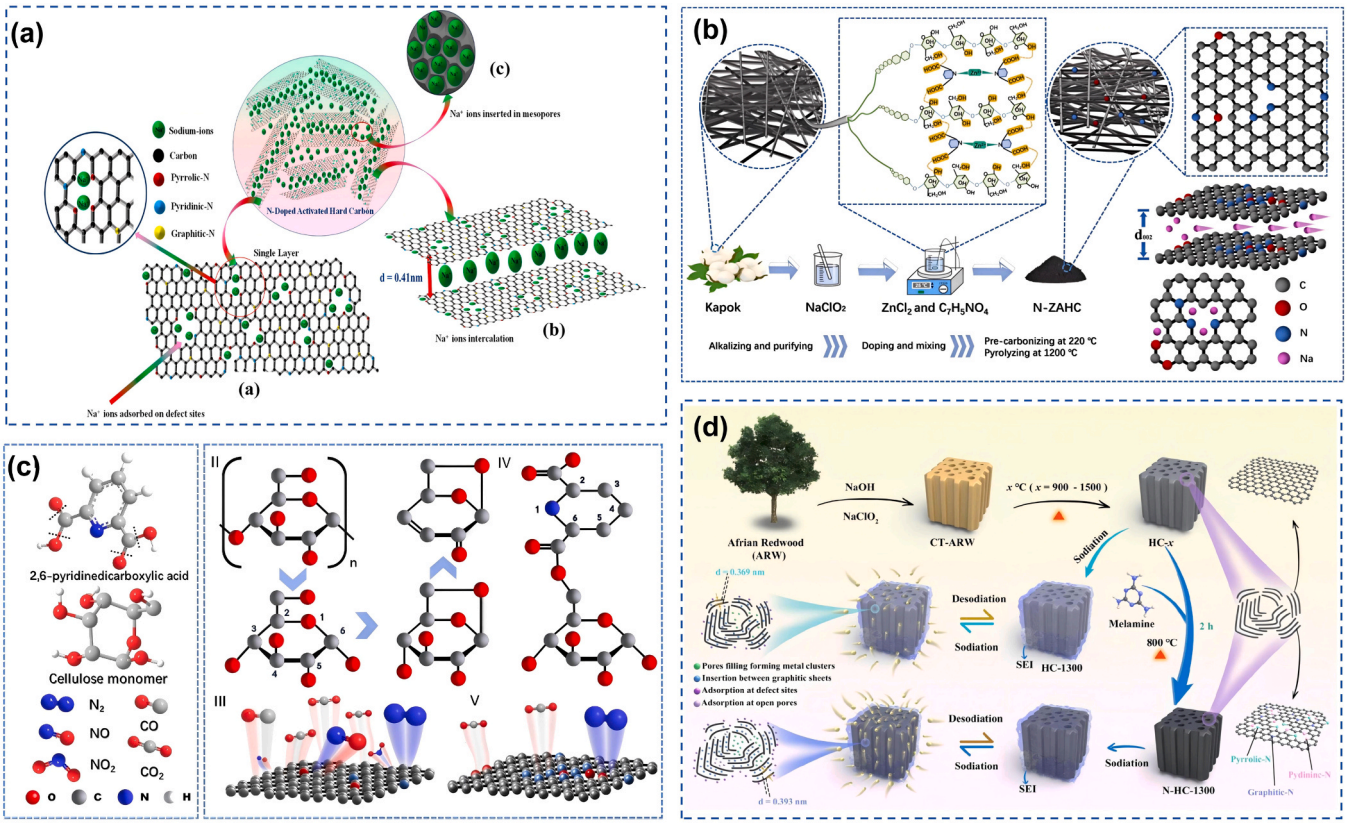

Fig. 13. Mechanisms of N doping on the structural modulation of hard carbon. (a) Structure-activity relationship between pyridinic N/pyrrolic N configurations and sodium storage mechanisms(Patel et al., 2024); (b) Synthesis process of nitrogen-rich hard carbon via the "pre-crosslinking-assisted pyrolysis" strategy(Zhang et al., 2024b); (c) Structural evolution mechanism during the pyrolysis of 2,6-pyridinedicarboxylic acid and kapok cellulose(Zhang et al., 2024b); (d) N doping process using African rosewood as the hard carbon precursor(Huang et al., 2025).

"high-temperature carbonization–secondary reconstruction" strategy (post-treatment method): first constructing a stable carbon skeleton at high temperature, then introducing a nitrogen source for surface and near-surface doping (Fig. 13d). In this pathway, local distortion induced by N atoms on the existing skeleton promotes closed-pore formation, while surface-enriched pyridinic/pyrrolic nitrogen modulates SEI composition via Na–N interactions, inducing a stable interface layer rich in Na_3N, thereby synergistically enhancing both plateau capacity and initial Coulombic efficiency.

The above comparison reveals a key rule: the beneficial effect of N doping depends not simply on the total doping amount but jointly on doping timing and nitrogen configuration. The one-step method favors maximizing defect adsorption, whereas the post-treatment method optimizes closed-pore structures and interfacial chemistry on a stable carbon skeleton. The core challenge of N doping lies in the uncontrollable loss and configuration transformation of nitrogen species during high-temperature carbonization, which hinders precise pre-design of active site density and type. Future research should focus on strategies

for targeted stabilization of nitrogen configurations to achieve a transition from "empirical doping" to "on-demand design."

5.1.1. P doping

Unlike N doping, which primarily modifies the carbon skeleton through electronic effects, P doping is distinguished by its pronounced geometric distortion effect. The significantly longer P–C bond (compared to C–C) causes the substitutional P–(C_3) configuration to form local "protrusion" structures on the carbon plane, thereby geometrically expanding the interlayer spacing of graphitic microcrystallites (Wu et al., 2018a). Concurrently, the valence electronic structure of P atoms effectively increases the density of states near the Fermi level, transitioning the material from semiconducting to highly conductive or even metallic-like behavior. This dual geometric and electronic amplification makes P doping a powerful strategy for enhancing the rate performance of hard carbon.

A cross-comparison of two representative P doping pathways further reveals their structure–activity differences. The high-content bulk doping pathway (Yan et al., 2021) focuses on intrinsically reconstructing the conductive network of the carbon skeleton (Fig. 14a, b). By uniformly embedding an ultra-high proportion of P under oxygen-free conditions, the carbon matrix acquires metallic-like conductivity, the interlayer spacing is significantly expanded, and the sodium storage kinetics shift from diffusion-controlled to surface-capacitive mechanisms, thereby maintaining considerable capacity even at ultra-high current densities. The plasma-assisted doping pathway (Kim et al., 2020) (Fig. 14c) places greater emphasis on defect engineering and the construction of surface active sites. Leveraging the synergistic effect of topological defects induced by high-energy plasma on the carbon surface together with moderate P doping, the sodium storage behavior becomes almost completely dominated by fast surface-capacitive processes, resulting in an extremely long cycle life.

The above comparison indicates that the beneficial mechanism of P doping strongly depends on doping content and distribution depth: high-content bulk doping reshapes the conductive network, making it suitable for ultra-high rate scenarios; low-content surface doping optimizes the capacitive contribution, making it suitable for ultra-long cycle life requirements. However, the large-scale application of P doping still faces a key bottleneck: the P–C bond is highly sensitive to oxygen, readily oxidizing to form electrochemically inert PO_x species that not only consume active P sites but may also block ion transport channels. Achieving a high proportion of substitutional P doping under a controlled atmosphere while suppressing inert phase formation is therefore a key future research direction.

5.1.2. S doping

Unlike N and P doping, which primarily affect the electronic structure of the carbon skeleton, S doping exhibits a unique dual physical–chemical functionality. At the physical level, the decomposition and release of sulfur species at high temperatures generate a gas-phase etching effect, constructing microporous–mesoporous composite networks within the carbon matrix (Fig. 15a, b), shortening Na^+ diffusion paths and improving kinetic behavior. At the chemical level, the thiophenic sulfur configuration (C–S–C) modulates the local electronic density of states, significantly influencing the adsorption strength of Na^+ at defect sites and thereby tuning the reversibility of sodium storage.

Comparing bulk doping and surface modification pathways clearly reveals the differentiated mechanisms of S doping. The bulk etching-doping pathway is characterized by the in-situ release of sulfur vapor during pyrolysis (Sun et al., 2025a). As sulfur species escape, they simultaneously create pores and achieve thiophenic doping; the resulting hierarchical pore system substantially enhances ion transport efficiency, and the sodium storage behavior transitions from bulk diffusion-controlled to fast surface-capacitance-dominated, thereby delivering outstanding rate performance (Fig. 15c). In contrast, the surface sulfurization pathway employs post-treatment techniques such as chemical vapor deposition (de Tomas et al., 2023) to form stable C–S–C covalent bonds on the surface of pre-carbonized hard carbon

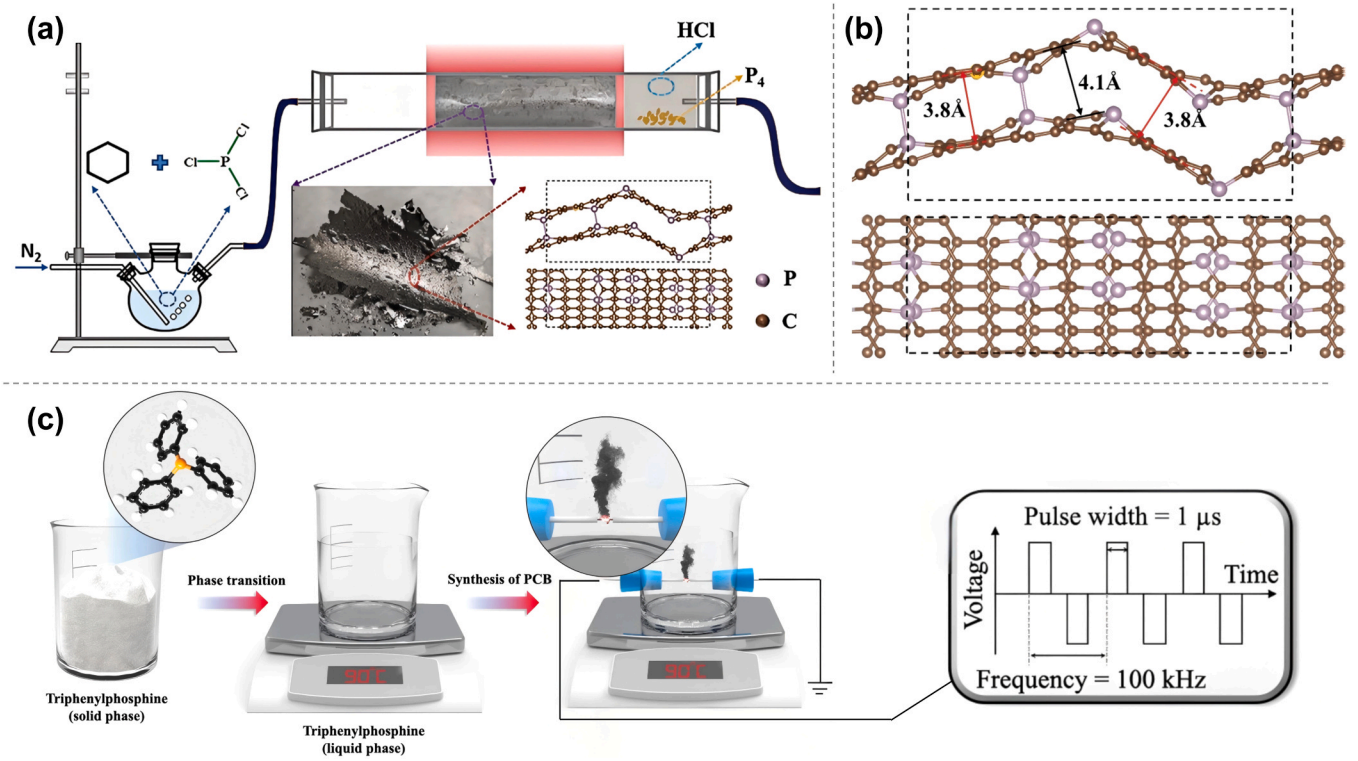

Fig. 14. Fabrication processes and theoretical structures of P-doped hard carbon. (a-b) Schematic diagram of the apparatus for synthesizing hard carbon via the oxygen-free liquid-phase precursor bubbling method and the corresponding rational structure based on theoretical calculations(Yan et al., 2021); (c) Fabrication process of the solution plasma process (SPP)(Kim et al., 2020).

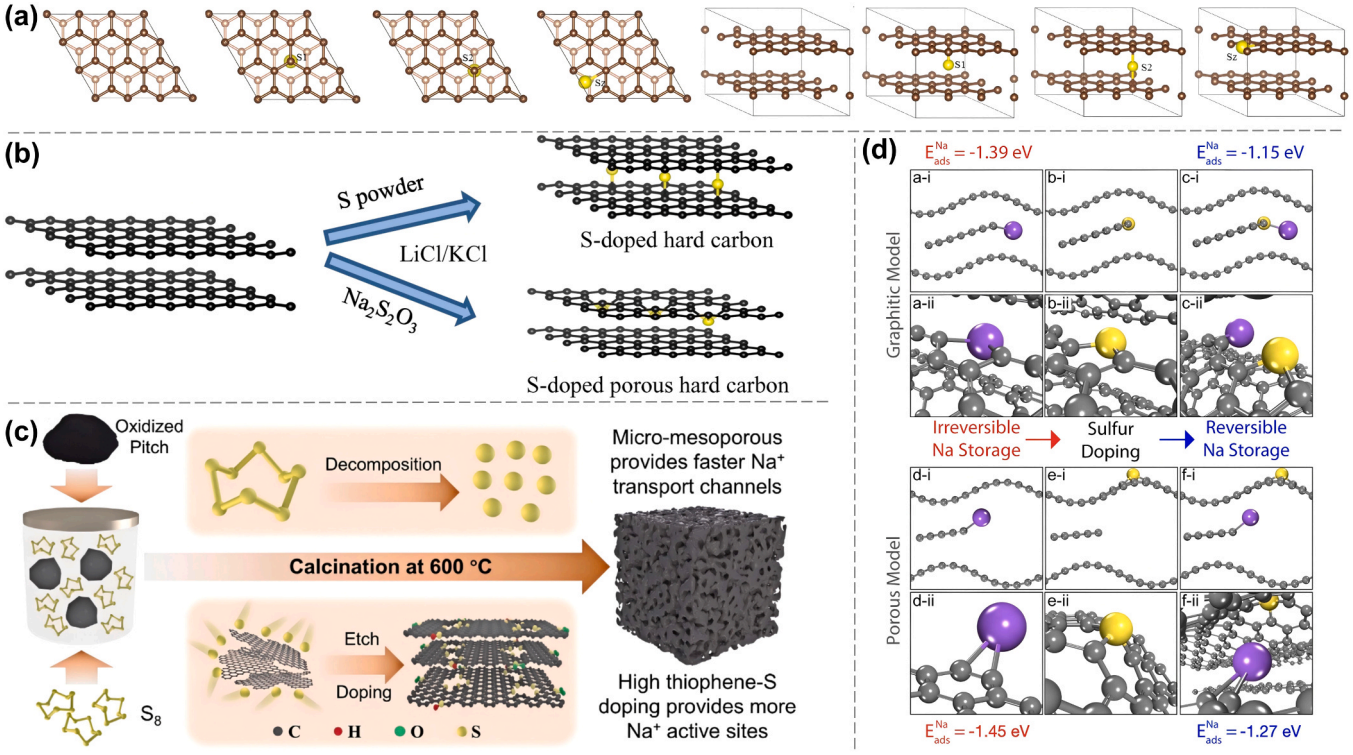

Fig. 15. Mechanisms of S doping on electrochemical performance. (a) Crystal structure models of different S doping configurations(Hong et al#, 2018); (b) Hard carbon structures derived from different sulfur sources(Hong et al#, 2018); (c) Schematic illustration of porous carbon preparation via in-situ gas-phase etching(Sun et al#, 2025a); (d) Atomic-scale mechanism of S doping-induced transition of Na^+ storage from irreversible to reversible behavior(de Tomas et al#, 2023).

without disrupting the bulk graphitic microstructure (Fig. 15d). The core value of this pathway lies in its precise thermodynamic modulation of Na^+ adsorption energy at edges and defect sites—by destabilizing strong adsorption sites, it converts a portion of irreversibly trapped Na^+ into a reversibly de/intercalatable state, thereby significantly enhancing the initial Coulombic efficiency while maintaining a relatively high capacity.

The main challenges currently facing S doping are as follows. In bulk doping, the synergistic control between sulfur content and closed-pore development remains immature; excessive sulfur release may lead to over-development of open pores, compromising the initial Coulombic efficiency. Surface sulfurization, in contrast, requires a more delicate balance between passivating strong adsorption sites and retaining sufficient active sites. Achieving targeted processing of sulfur doping location and configuration according to the desired performance is therefore a core objective for future research in this direction.

5.2. *Multi-element doping*

Building on single-element doping, co-doping with two or more heteroatoms aims to overcome the performance ceiling of single-element doping through synergistic effects among different elements. Typical combinations include N/P, N/S, and N/O (Fig. 16).

Comparing different co-doping systems, the strength of the synergistic effect strongly depends on the compatibility of the elemental combination and the preparation process. N/P co-doping excels at balancing capacity and rate capability, while N/S co-doping offers advantages in constructing hierarchical pore structures and modulating surface chemistry. However, multi-element doping is not simply a performance enhancer. When multiple heteroatoms coexist, they may compete for limited doping sites or interfere with each other's electronic structure processing, causing actual results to deviate from expectations. Furthermore, introducing multi-element precursors often significantly increases process complexity and cost.

In summary, by rationally introducing multiple heteroatoms (e.g., N, P, S) and precisely processing their proportions and distributions, synergistic optimization can be achieved among key performance indicators including discharge capacity, rate capability, cycling stability, and initial Coulombic efficiency (ICE) (Fig. 17). However, its potential limitations remain: the synergistic mechanisms are unclear, competitive relationships among elements are difficult to predict, and the feasibility of process scale-up is questionable. Future research should shift from "trial-and-error combinations" to "on-demand design"—deducing functional combinations from target sodium storage behavior and then precisely screening element pairs and their ratios. Only then can multi-element doping truly move toward rational design.

6. Interfacial engineering

6.1. *Surface coating*

Interfacial engineering involves forming an SEI layer on the electrode surface to prevent further electrolyte decomposition, enhance interfacial stability, and protect the electrode material from damage, thereby improving the cycling performance of sodium-ion batteries.

Lu et al. (Lu et al., 2019) effectively enhanced the initial Coulombic efficiency, reversible capacity, and cycling stability of hard carbon anodes in sodium-ion batteries using an ALD-Al_2O_3 coating method (Fig. 18a). Compared to bare electrodes, the non-conductive Al_2O_3 deposited film induced the formation of an SEI layer with more organic components, preventing electrolyte penetration and reducing side reactions, thus achieving stable cycling performance. Moreover, the Al_2O_3 film effectively lowered interfacial resistance, allowing more sodium ions to intercalate into the graphene layers and resulting in a significant increase in plateau capacity. This aligns well with the "adsorption-insertion" mechanism (Cao et al., 2012), where slope capacity is attributed to Na^+ adsorption at defects and pores, and plateau capacity is associated with Na^+ intercalation into the carbon layers.

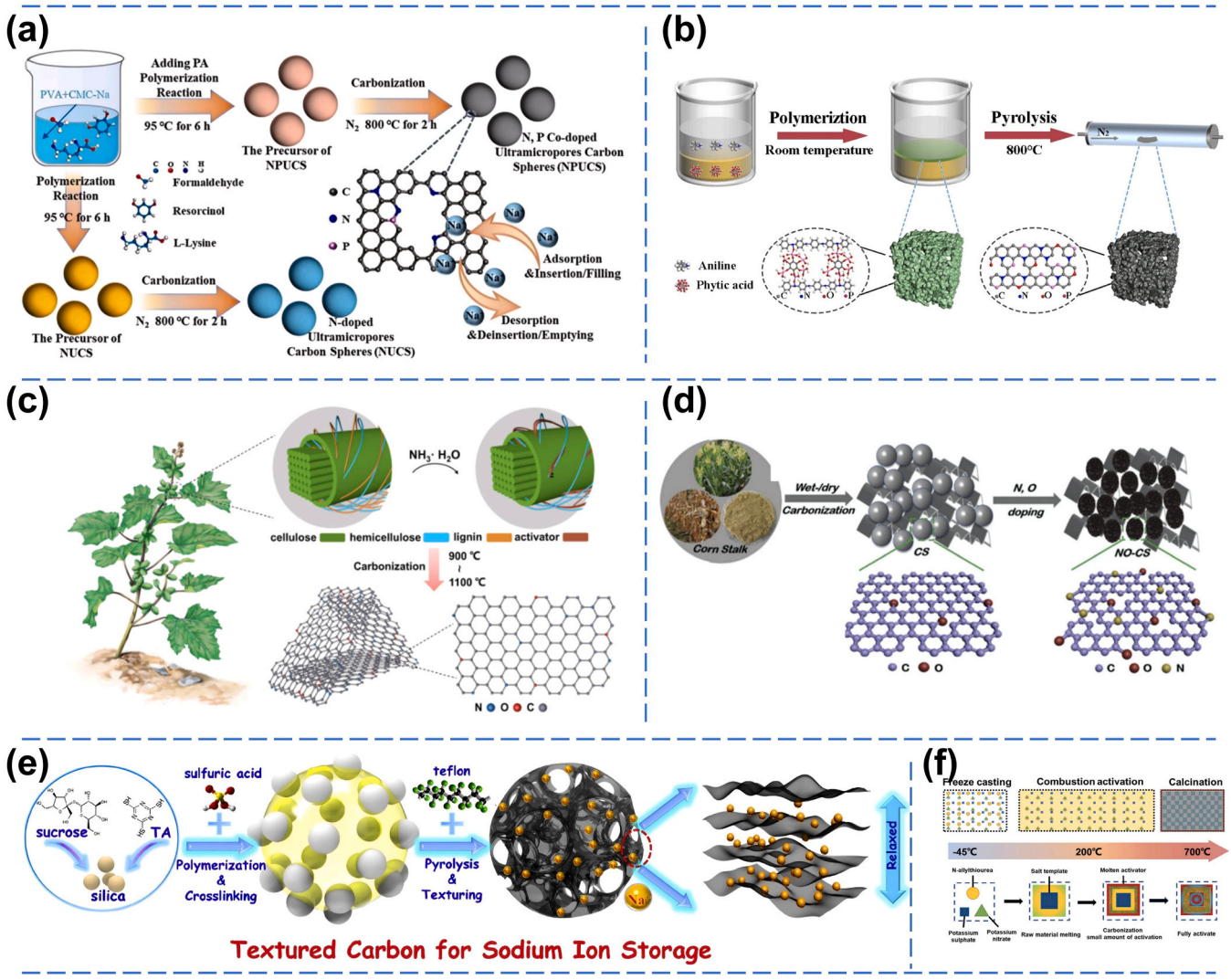

Fig. 16. Preparation processes for multi-element doped hard carbon. (a-b) Fabrication process of N/P dual-doped hard carbon precursors(Wu et al., 2022a; Wu et al., 2024b); (c-d) Fabrication process of N/O dual-doped hard carbon precursors(Shi et al., 2022; Zhang et al., 2019); (e-f) Fabrication process of N/S dual-doped hard carbon precursors and the novel combustion activation strategy(Pei et al., 2020; Zhang et al., 2024a).

Yu et al. (Yu et al., 2022b) modified the hard carbon surface using 2, 2-dimethylvinylboronic acid (DEBA) (Fig. 18b). DEBA contains carbon–carbon double bonds and B-OH functional groups. During liquid-phase coating, the B-OH groups react with –COOH and –OH groups on the hard carbon, forming stable chemical bonds that tightly adhere to the carbon surface. This prevents excessive electrolyte decomposition, thereby enhancing sodium storage performance.

Material compositing primarily improves battery electrochemical performance by modifying the interfacial properties of electrode materials. Specifically, composites can enhance sodium storage mechanisms and diffusion kinetics, thus boosting overall battery performance. Li et al. (Li et al., 2024) synthesized a hard carbon/soft carbon composite using a layer-by-layer and confinement effect strategy (Fig. 18c). The resulting composite featured a comprehensive conductive network, high defect density, and sufficient interlayer spacing, leading to outstanding specific capacity and excellent rate performance.

6.2. Functional group processing

The grafting of functional groups can promote both diffusion-controlled processes and surface-limited capacitive processes.

The sol-gel method can effectively control the microstructure and surface functional groups of materials, thereby significantly improving the cycling stability and rate performance of sodium-ion batteries. Zhang et al. (Zhang et al., 2020) synthesized nanoscale porous carbon spheres via the sol-gel method using resorcinol (Fig. 19a). The prepared electrode retained a capacity of 232.6 mAh g^{-1} after 100 cycles at 200 mA g^{-1} , and the KFSI-DME electrolyte system effectively increased the initial Coulombic efficiency to 68.2%. Chen et al. (Chen et al., 2017) developed nitrogen-rich, micro-crosslinked, hierarchically porous microsphere hard carbon from chitin using the sol-gel method (Fig. 19b). This structure facilitated sodium ion de/intercalation and improved rate performance, as evidenced by a discharge capacity of 156 mAh g^{-1} maintained at 18 C, demonstrating excellent cycling stability and rate capability.

Pre-oxidation treatment introduces specific functional groups onto the material surface and forms a stable SEI layer, thereby not only enhancing the structural stability and electrochemical performance of electrode materials for sodium-ion batteries but also further optimizing overall battery performance by modulating the electronic and phase structures of the material. Chen et al. (Chen et al., 2024) performed glucose grafting and carbonization on the surface of pristine powdered pitch (Fig. 19c). After carbonization, the glucose molecules formed a thin, low-defect carbon layer that reduced the specific surface area,

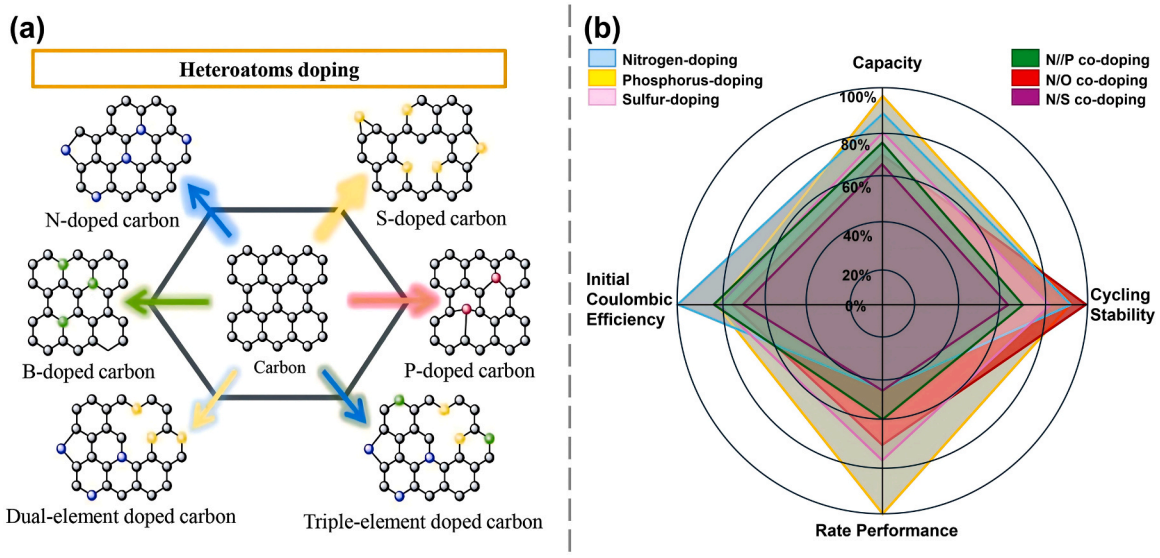

Fig. 17. (a) Structural changes in hard carbon under different heteroatom doping configurations (Chen et al., 2018); (b) Influence patterns of heteroatom doping on electrochemical performance. The four performance dimensions are normalized to 100% based on the optimal values across all doping systems: capacity normalized to 401.7 mAh g^{-1}; cycling stability normalized to 96.8% capacity retention after 2000 cycles; initial Coulombic efficiency normalized to 90.1%; rate capability normalized to 397.1 mAh g^{-1} at 10 A g^{-1}; plateau capacity normalized to 350.1 mAh g^{-1}.

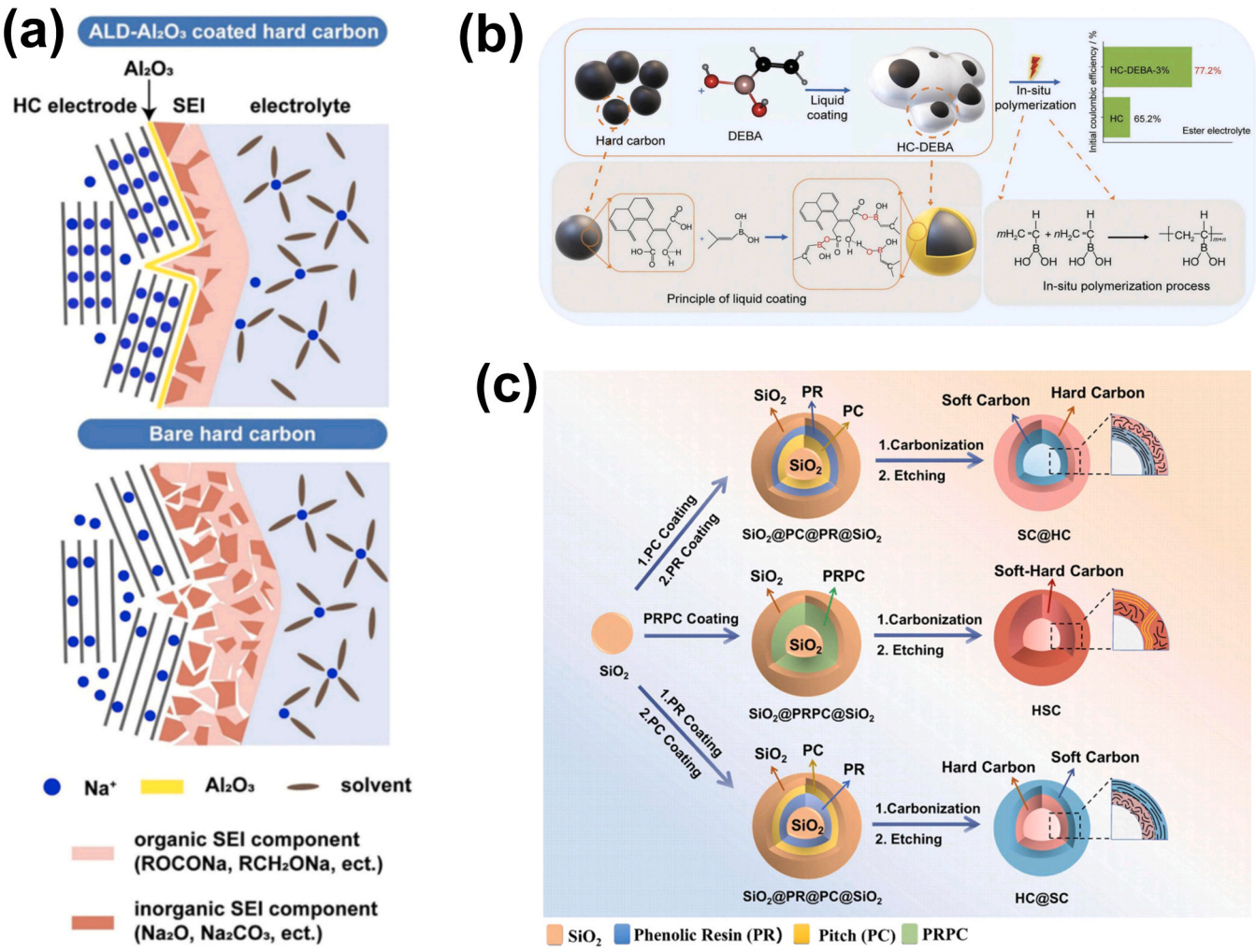

Fig. 18. Schematic diagrams of surface coating processes. (a) Schematic illustration of the effect of ALD-Al2O3 coating on hard carbon(Lu et al., 2019); (b) Schematic diagram of the surface modification process for hard carbon using 2,2-dimethylvinylboronic acid (DEBA)(Yu et al., 2022b); (c) Schematic illustration of the synthesis process for hard carbon/soft carbon-based hollow carbon spheres(Li et al., 2024).

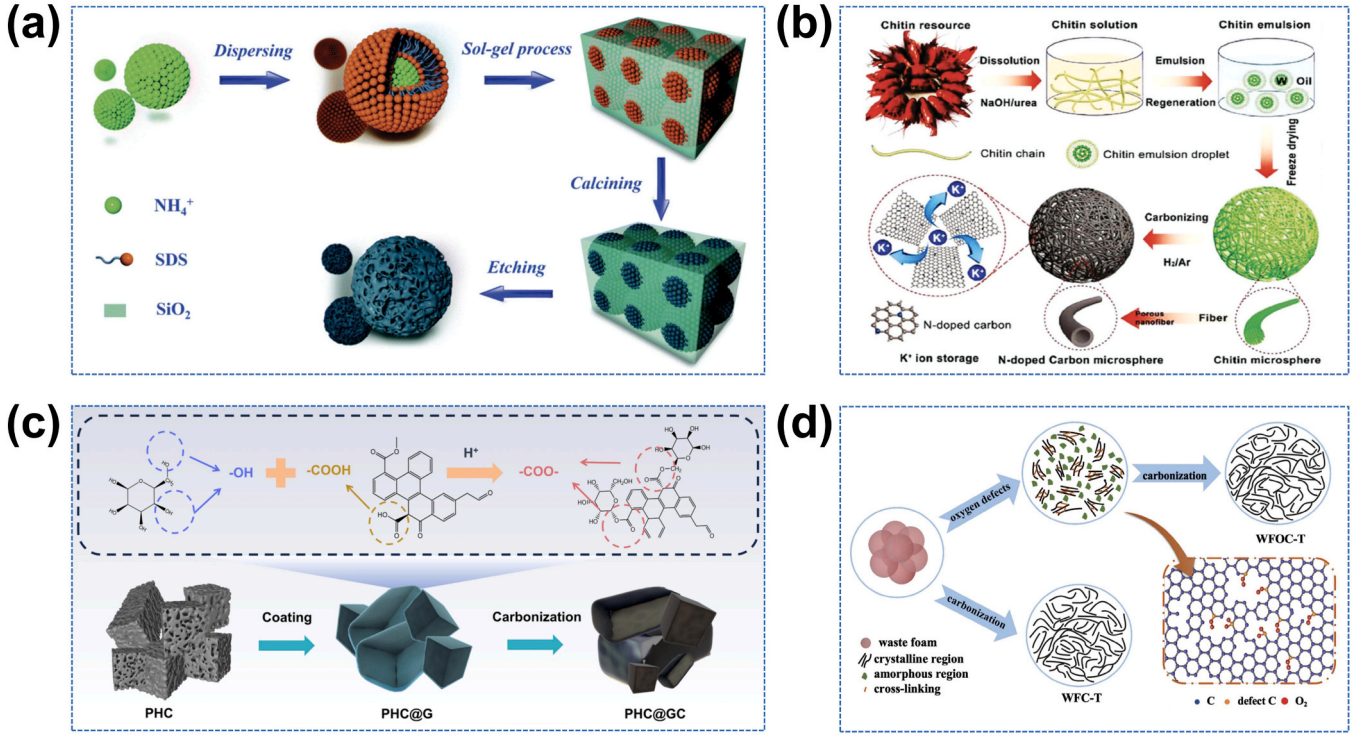

Fig. 19. (a) Schematic illustration of the synthesis of nanoscale porous spherical carbon using the sol-gel method(Zhang et al., 2020); (b) Schematic diagram of the synthesis of nitrogen-rich microsphere hard carbon from chitin(Chen et al., 2017); (c) Process of glucose grafting and carbonization on the hard carbon surface to form a thin core-shell structure(Chen et al., 2024); (d) Schematic illustration of the synthesis of waste foam-derived carbon structure(Ji et al., 2025).

adjusted the pore structure, and enhanced sodium ion transport, resulting in high specific capacity and high initial Coulombic efficiency. Ji et al. (Ji et al., 2025) introduced abundant oxygen-containing groups as cross-linking active sites through an air oxidation process to obtain a stable carbon precursor (Fig. 19d). Subsequent high-temperature carbonization produced hard carbon with a high degree of disorder and moderate interlayer spacing. The optimized waste foam-derived hard carbon exhibited a reversible specific capacity of 308 mAh g^{-1} at 20 mA g^{-1} , an initial Coulombic efficiency of 90.1%, and a capacity retention of 85% after 100 cycles, demonstrating excellent initial Coulombic efficiency and cycling stability.

7. Morphology regulation

The template method uses hard templates to prepare porous carbon materials with specific pore structures. Its advantage lies in the precise control over pore size and distribution, yielding porous carbon with high specific surface area and well-developed pore architecture, thereby

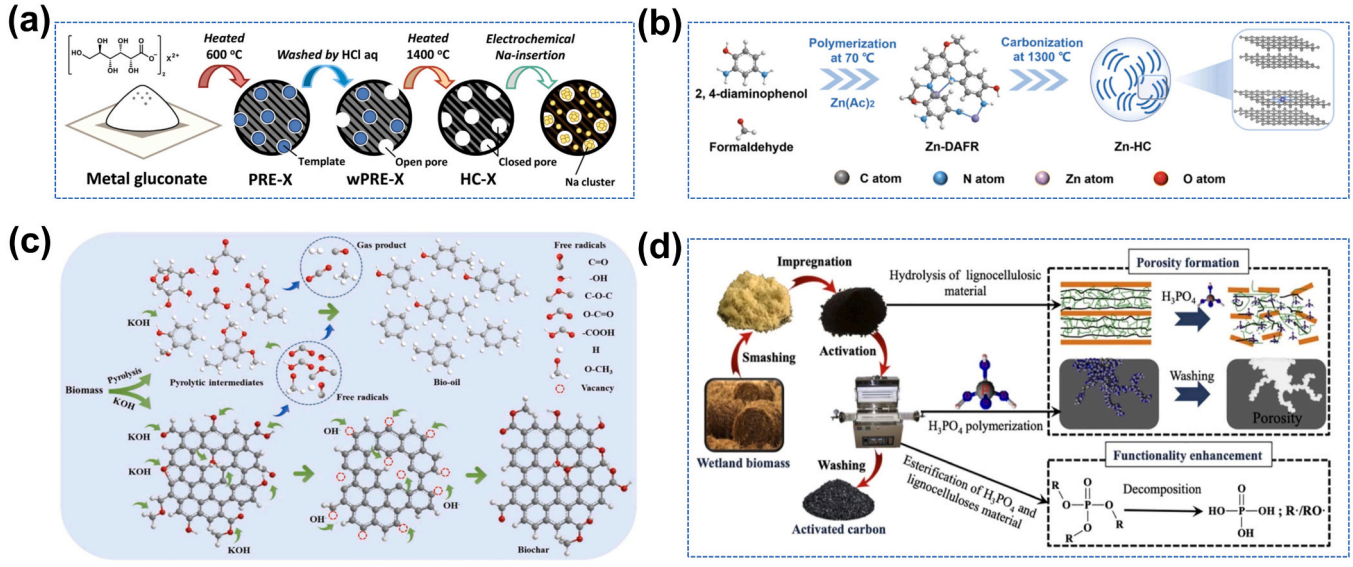

Fig. 20. (a) Schematic illustration of hard carbon synthesis via the template method(Igarashi et al., 2023); (b) Schematic diagram of atomic Zn modulating the morphological structure of hard carbon(Lu et al., 2023b); (c) Chemical reaction pathways during KOH activation(Chen et al., 2020); (d) Scheme for the production of porous carbon from biomass via H3PO4 activation(Liu et al., 2021a).

enhancing the electrochemical performance of hard carbon materials.

Igarashi et al. (Igarashi et al., 2023) employed a template method to prepare hard carbon materials, using gluconate as the template carbon precursor. The process involved pre-carbonization at 600 °C, subsequent acid leaching, and final heating in an inert atmosphere to obtain hard carbon featuring graphitic-like domains and closed nanopores (Fig. 20a). The resulting hard carbon exhibited high discharge capacity and excellent cycling stability. Lu et al. (Lu et al., 2023b) used 2,4-diaminophenol-formaldehyde resin (DAFR) as the carbon and nitrogen precursor, and zinc acetate as the zinc precursor, to synthesize Zn-HC material via a two-step method (Fig. 20b). The obtained material demonstrated excellent low-temperature performance at −40 °C, and the assembled Zn-HC= |NVP full cell exhibited a high energy density (323 Wh kg^{-1}) and high power density (7.02 kW kg^{-1}).

The activation method enhances the pore structure and surface properties of hard carbon materials by increasing their specific surface area and porosity through chemical or physical means. It is also commonly employed to improve the performance of hard carbon materials in electrochemical energy storage.

Chen et al. (Chen et al., 2020) investigated the chemical reaction pathways during biomass pyrolysis using KOH as an activator (Fig. 20c). Between 400 and 700 °C, KOH reacted with oxygen-containing species to form K_2CO_3, which further converted into K_2O at 800 °C. These processes increased the oxygen content and porosity of the biomass-derived hard carbon. The reactions of KOH with various intermediates promoted the formation of non-methoxylated phenols and hydrocarbons, while inhibiting the generation of acetic acid, oxygen-containing species, and methoxylated phenols, thereby significantly improving the quality of the bio-oil. Liu et al. (Liu et al., 2021a) summarized a strategy for converting wetland biomass into porous carbon via H_3PO_4 activation (Fig. 20d). During the impregnation stage, H_3PO_4 hydrolyzed the biomass, depolymerizing lignocellulose into low-molecular-weight sugar monomers and forming new polymeric phosphate structures through phosphorylation. In the activation stage, H_3PO_4 acted as a dehydrating agent, promoting the carbonization and aromatization of lignocellulosic precursors at relatively low temperatures. Depending on the heating temperature, H_3PO_4 species could transform into different polycondensed forms.

8. Discussion on the applicability of modification strategies

8.1. Applicability of modification strategies to biomass-derived hard carbon

Synthesizing Sections 5–7, the effects of the same modification method on model hard carbon versus real biomass-derived hard carbon exhibit significant differences. Therefore, discussing the applicability of modification strategies to biomass-derived hard carbon is crucial.

Among these, N doping has been validated in biomass-derived systems to enhance slope capacity, initial Coulombic efficiency (ICE), and plateau capacity. This can be achieved by utilizing the intrinsic nitrogen-containing components of biomass or through post-treatment methods (e.g., ammonia or melamine thermal treatment) (Huang et al., 2025; Li et al., 2025b). In contrast, high-content P and S doping remain largely confined to model systems (e.g., triphenylphosphine-derived carbon) and exhibit low transferability to biomass-derived carbons, manifesting as low doping efficiency, susceptibility to oxidation forming inert PO_x/SO_x species, and excessive pore formation that compromises ICE. Low-concentration surface doping is recommended to moderately improve rate performance (Liang et al., 2025; Liu et al., 2025b).

Furthermore, surface coating (e.g., ALD, CVD, liquid-phase coating) has been proven to enhance ICE and cycling stability in biomass-derived hard carbon. Mild liquid-phase or gas-phase methods should be prioritized to construct uniform coating layers that accommodate the high specific surface area of biomass-derived hard carbon (Wang and Su, 2021). Functional group processing (e.g., pre-oxidation treatment) has been validated in biomass cases (such as waste foam and bamboo fibers) to improve reversible capacity and ICE (Chen et al., 2024).

In terms of morphology regulation, activation methods (e.g., KOH, H_3PO_4) have been widely applied to biomass-derived hard carbon, enhancing specific surface area and rate performance. However, the activation degree must be controlled to avoid compromising ICE, making this the preferred approach for large-scale production (Hong et al., 2014; Yanilmaz et al., 2025). The template method exhibits low transferability to biomass-derived systems, primarily limited by poor compatibility between templates and biomass precursors and the propensity for framework collapse. It is only applicable to biomass that has undergone pretreatment such as delignification, allowing precise control of pore structures to improve rate performance, albeit at higher cost (Saikia et al., 2023).

8.2. Applicability of modification strategies to full cells

Significant progress has been made in evaluating modification strategies for hard carbon anodes in half-cells. However, transitioning from half-cell to full-cell is not a simple performance translation. In half-cells, the sodium metal counter electrode provides an unlimited and continuously stable sodium source, masking the true effects of modification strategies on sodium consumption, interfacial stability, and anode-cathode compatibility. Therefore, whether modification strategies that perform well in half-cells remain effective in full-cells urgently requires systematic evaluation.

In terms of heteroatom doping, precise processing of surface defects and oxygen heteroatoms has demonstrated applicability in full-cells. Liu et al. used methane-assisted post-treatment to increase the half-cell ICE of commercial hard carbon from 80% to 90% and the reversible capacity from 270 to 310 mAh g^{-1} , and assembled full-cells with a $Na_3V_2(PO_4)_3$ cathode to validate the strategy (Liu et al., 2025a). However, excessive doping can increase surface side reactions, leading to excessive sodium consumption in full-cells and reducing ICE and cycling stability. Therefore, heteroatom doping in full-cells should shift from "capacity maximization" to "sodium source optimization."

Furthermore, surface coating and SEI design exhibit particularly outstanding applicability to full-cells, significantly enhancing ICE and cycling stability. Zhang et al. constructed a phosphide layer on bamboo powder-derived hard carbon, inducing the formation of a Na_3P-rich SEI. Theoretical calculations indicated that Na_3P can reduce the solvent coordination number, achieving a lower desolvation energy barrier and faster Na^+ diffusion. The full-cell assembled with this anode and a $Na_3V_2(PO_4)_3$ cathode delivered 78 mAh g^{-1} at 10 C, and a pouch cell cycled stably for 1000 cycles at 0.5 C (Zhang et al., 2025a). Interfacial engineering is even more critical in full-cells than in half-cells because the electrolyte amount is limited and the cathode is sensitive; thus, a stable SEI is a prerequisite for long-term cycling (Pei et al., 2025).

Through morphology regulation strategies, precise construction of closed-pore structures can influence the output voltage and energy density of full-cells. Yan et al. adopted a synergistic strategy combining closed pores and interfacial engineering, using waste polyolefin-derived activated carbon as a precursor, and assembled a full-cell with an O3-$NaNi_{1/3}Fe_{1/3}Mn_{1/3}O_2$ cathode, achieving an energy density as high as 307.3 Wh kg^{-1} (Yu et al., 2025). However, excessive pore formation via activation methods increases the proportion of open pores, reducing ICE. While the template method offers controllable pore structures, it suffers from high cost and process complexity. Therefore, morphology regulation targeting full-cells should pursue a high closed-pore volume while strictly controlling the proportion of open pores.

Through this discussion of the applicability of modification strategies to biomass-derived hard carbon and full-cells, this work not only identifies directions for future research on modifying biomass-derived hard carbon but also lays a foundation for its application in full-cells and industrialization.

9. Industrialization progress and challenges

With the accelerating industrialization of hard carbon anodes for sodium-ion batteries, companies are rapidly expanding production capacity by leveraging their respective advantages in raw materials and processing technologies. Shengquan Group, relying on its integrated biorefinery advantages, has adopted a unique "biomass-resin" composite route. By extracting hemicellulose and lignin from agricultural and forestry residues such as corncobs and straw, the company produces furan/phenolic resins in-house as precursors, effectively addressing the challenge of poor consistency in biomass feedstocks. Its planned annual production capacity has reached the 100,000-ton scale (SECURITIES, 2022). BTR has adopted a multi-technology roadmap in the sodium-ion battery field, focusing on coconut shell- and starch-based hard carbon. Its latest product, "Tanna 350," delivers a specific capacity of 350 mAh g^{-1} with an initial Coulombic efficiency (ICE) approaching 90%, and the company plans to expand production to 50,000 tons per year by 2025 (Materials, 2023). Kuraray has focused on overcoming the hygroscopicity challenge of biomass-derived hard carbon (KURANODE™). Its products are compatible with water-based binders, significantly lowering the barrier to battery manufacturing. Stora Enso is committed to building a localized European supply chain, developing Lignode® hard carbon from lignin—a paper industry by-product—emphasizing low carbon footprint and sustainability, and actively advancing industrial collaborations with multiple battery manufacturers (Zlatev, 2024).

Addressing the structural stability of biomass and resin precursors during pyrolysis, cross-linking modification has become key. Taking relevant patents from BTR (e.g., involving maleic anhydride esterification cross-linking) as an example, a rigid three-dimensional network is constructed by introducing cross-linking agents that react with hydroxyl groups in the precursor. This process not only suppresses graphitization tendency and foaming at high temperatures, significantly improving carbon yield, but also ensures the stability of the turbostratic structure at the microscopic level, thereby enhancing sodium storage capacity. Furthermore, low ICE can be addressed through pore engineering and surface modification. Advanced patented technologies (e.g., CVD surface coating) tend to construct a "core–shell structure": an amorphous carbon coating is formed on the hard carbon surface via chemical vapor deposition, sealing open surface pores to block electrolyte side reactions while retaining the abundant internal closed-pore structure for sodium storage. When combined with acid washing purification and low-oxygen control processes (such as those in Kuraray's patents), the oxygen content can be reduced below 0.25%, substantially lowering irreversible capacity loss and improving cycle life.

Despite rapid progress in the industrialization of hard carbon anodes for sodium-ion batteries, numerous challenges remain. Differences in the composition and structure of various biomass precursors (e.g., cellulose/lignin ratio) lead to variations in the electrochemical performance of the resulting hard carbons, causing significant product performance fluctuations and a lack of unified industrial performance standards. This situation also increases material processing costs and may involve environmentally unfriendly steps, undermining the low-cost and environmental advantages of sodium-ion batteries. Furthermore, the industry still lacks dedicated reactors tailored to the specific pyrolysis kinetics of hard carbon. When existing reactors are used for processing precursor materials at the kiloton scale, tar and volatile redeposition can cause surface pore blockage, compromising performance.

To promote the industrialization of biomass-derived hard carbon materials, additional practical performance metrics should be considered, including mass loading, tap density, volumetric capacity, initial Coulombic efficiency, average Coulombic efficiency during long-term cycling, presodiation strategies, electrolyte dependence, binder compatibility, full-cell compatibility, and cost per kilowatt-hour (Table 4).

As shown in Table 4, biomass-derived hard carbon materials still face numerous challenges in transitioning from laboratory to industrialization. Moreover, these challenges are not isolated performance shortcomings but rather coupled systemic contradictions. The greatest limitation of current research is the excessive focus on pursuing a "local optimum" of a single metric while neglecting the comprehensive material performance required for industrialization. For example, high plateau capacity requires fully developed closed pores, which in turn demands that carbon layers curl and fold at high temperatures, often leading to complex particle morphologies and low tap density. Recently, researchers have begun to recognize this issue. Hu et al. (Hu et al., 2025) employed a mass-transfer-enhanced pre-oxidation strategy to process pitch-based hard carbon, successfully achieving a synergistic improvement in closed-pore ratio (30.29%) and high tap density (0.9 g cm^{-3}). However, their work used carefully designed pitch precursors and pre-oxidation processes; the complex composition and batch-to-batch variations of biomass precursors challenge the direct transferability of this strategy.

Similar to tap density is the choice of electrolyte. Ether-based electrolytes exhibit significant advantages in low-temperature applications due to their high ionic conductivity and low desolvation energy (Deng et al., 2025). Although ester-based electrolytes are stable at high voltages, they suffer from sluggish interfacial ion diffusion and limited sodium nucleation kinetics. Thus, electrolyte selection for industrial applications must balance both anode interfacial kinetics and cathode voltage windows.

Table 4
Biomass-derived hard carbon anodes from laboratory to industrialization: key practical metrics, current status, and industrialization requirements.

Metric category	Specific parameter	Laboratory half-cell characteristics	Industrialization characteristics/ requirements	Ref.
Electrode engineering	Mass loading	1–2 mg cm^{-2}	> 5 mg cm^{-2}	(Raj and Franco, 2025; Zheng et al., 2022)
	Tap density	0.4–0.7 g cm^{-3}	> 0.9 g cm^{-3}	(Beda et al., 2021; Zhao et al., 2025)
	Volumetric capacity	150–250 mAh cm^{-3}	> 300 mAh cm^{-3}	(Beda et al., 2021)
Electrochemical performance	ICE	60–80%	> 85–90%	(Beda et al., 2021; Liu et al., 2025a; Pei et al., 2025)
	Cycling stability	90–95% (after 500 cycles)	> 92% (after 500 cycles)	(Beda et al., 2021; Liu, 2025; Pei et al., 2025; Zhang et al., 2025b)
Electrolyte compatibility	Ester-based electrolyte	Low ICE, limited plateau	High voltage stability, compatible with high-voltage cathodes	(Xu et al., 2023a; Yin et al., 2023)
	Ether-based electrolyte	High ICE, high plateau capacity	Poor high-voltage stability (<4.0 V)	(Xu et al., 2023a; Yin et al., 2023)
Presodiation	Presodiation method	Electrochemical/chemical presodiation	Cathode sodium compensation agent (most readily industrializable)	(Wang et al., 2025b; Yuan et al., 2025)
Manufacturing process	Electrode roll-pressability	Hard carbon particles prone to fracture	Maintain pore structure while being roll-pressable	(Beda et al., 2021; Raj and Franco, 2025)
	Binder compatibility	Mainly PVDF (NMP)	Mainly water-based binders (CMC/SBR)	(Jiao et al., 2024; Muruganantham et al., 2019)
Economics	Cost per kWh		$90–125 per kWh	(Dong, 2025)

Furthermore, the most prominent challenge in industrialization is high cost. Although the cost of sodium-ion batteries has decreased in recent years, their cost of $90–125 per kWh is still not competitive with that of lithium-ion batteries ($75–105 per kWh). Therefore, actively developing biomass-derived hard carbon materials is of great significance for the industrialization of sodium-ion batteries and will also help them approach the target of $40 per kWh (Dong, 2025).

10. Conclusions and outlook

This review systematically examines the structure–activity relationship between modification strategies and electrochemical performance of agricultural/forestry biomass-derived hard carbon anodes. Heteroatom doping (especially multi-element co-doping) tailors electronic structure and interlayer spacing, balancing capacity, rate capability, and cycling stability. Surface coating constructs a stable SEI layer, suppressing electrolyte decomposition and enhancing cycling stability. Morphology regulation optimizes pore architecture, improving ion transport and discharge capacity. These insights provide a roadmap for upgrading biomass residues into standardized hard carbon products.

Despite recent progress, research remains largely empirical. A predictable, systematic framework is lacking. We propose a three-stage roadmap:

Phase I (1–2 years): Build a hard carbon Materials Genome database. Collect and publicly release data on precursor composition (cellulose/lignin/hemicellulose ratios, ash, functional groups), processing parameters (temperature, ramp rate, hold time, atmosphere, pretreatment), microstructural parameters (interlayer spacing, defect density, closed-pore volume, open-pore surface area), and electrochemical performance (slope/plateau capacity, ICE, rate capability, cycle decay). The database should contain 200–300 high-quality, multi-variable entries with full metadata.

Phase II (2–3 years): Apply machine learning to model structure–activity relationships. Use random forest, XGBoost, or graph neural networks for forward prediction of plateau/slope capacity and ICE from precursor and processing inputs. Employ Bayesian optimization or active learning for inverse design (e.g., targeting ICE >88% and plateau capacity >250 mAh g^{-1}). Deliver an open-source "hard carbon design toolkit" to reduce trial-and-error costs.

Phase III (ongoing): Decouple mechanisms via advanced in-situ characterization. Simultaneously acquire in-situ SAXS (closed-pore filling), in-situ XRD (interlayer spacing), and in-situ Raman (defect evolution) in the same cell to answer: (i) Does closed-pore filling contribute to the low-voltage plateau (<0.1 V)? (ii) Is there a clear voltage boundary between intercalation and filling? (iii) How does defect evolution affect slope capacity over time/voltage? This will establish a causal chain from structural evolution to sodium storage mechanism to electrochemical response.

From an industrial perspective, commercial standards are essential for large-scale adoption. For cellulose-based hard carbon, target benchmarks include reversible capacity > 300 mAh g^{-1}, initial Coulombic efficiency (ICE) > 90%, and capacity retention > 90% after 1000 cycles. Low-cost, energy-efficient modification strategies should avoid high temperatures, multi-step chemical treatments, or expensive precursors, instead leveraging the intrinsic advantages of biomass. Regional feedstock optimization is recommended: bamboo (cellulose-rich) for high capacity, coconut shells (lignin-rich) for high plateau capacity, and straw/rice husks (defect-rich) for superior Na^+ adsorption. Research must also bridge the gap between half-cell evaluations and commercial full-cell requirements.

The structure–activity framework should be extended to other disordered carbons (porous carbon, activated carbon, soft/hard carbon composites), moving from single-material optimization to synergistic design of carbon material systems for sodium storage.

Life cycle assessment (LCA) confirms clear environmental benefits of biomass-derived hard carbon over graphite: global warming potential (GWP) reduced by 21–30%, and acidification/human toxicity potentials reduced by > 90%. Using agricultural/forestry residues as precursors significantly lowers environmental burden compared to sucrose or fossil-based feedstocks. Pyrolysis dominates laboratory-scale energy consumption (98%), but industrial scale reduces GWP dramatically. A cycle life exceeding 2000 cycles makes the life-cycle impact comparable to lithium-ion batteries. Process optimization (pyrolysis parameters, waste heat recovery) and large-scale production are key to further enhancing sustainability (Liu et al., 2024, 2021b; Peters et al., 2016).

In summary, the future of biomass-derived hard carbon anodes lies in shifting from "performance enhancement" to "predictable design." This will be achieved through a materials genome database, machine learning-driven modeling, in-situ characterization validation, low-cost industrialization, and cross-system verification of structure–activity relationships.

CRediT authorship contribution statement

Yugen Bao: Writing – original draft, Visualization, Validation, Methodology, Investigation, Data curation. **Tianyi Gao:** Writing – original draft, Visualization, Validation, Methodology, Investigation, Formal analysis, Data curation. **Luxiang Ma:** Writing – review & editing, Supervision, Methodology, Investigation, Funding acquisition, Conceptualization. **Yan Zhao:** Writing – review & editing, Investigation. **Hongli Su:** Writing – review & editing, Supervision, Methodology, Investigation, Conceptualization.

Declaration of Competing Interest

The authors declare that they have no known competing financial interests or personal relationships that could have appeared to influence the work reported in this paper.

Acknowledgment

This work was supported by the Qinghai Provincial Key R&D and Transformation Program (Grant No. 2025-QY-814), the Open Project of Salt Lake Chemical Engineering Research Complex at Qinghai University (Grant No. 2025-DXSSKF-12), and the Qinghai Provincial Major Science and Technology Special Project (Grant No. 2025-SF-A2). The APC was funded by the TU Delft Library.

Data availability

Data will be made available on request.

References

Agrawal, A., Janakiraman, S., Biswas, K., Venimadhav, A., Srivastava, S.K., Ghosh, S., 2019. Understanding the improved electrochemical performance of nitrogen-doped hard carbons as an anode for sodium ion battery. Electrochim. Acta 317, 164–172.
Alvin, S., Cahyadi, H.S., Hwang, J., Chang, W., Kwak, S.K., Kim, J., 2020. Revealing the Intercalation Mechanisms of Lithium, Sodium, and Potassium in Hard Carbon. Adv. Energy Mater. 10.
Alvin, S., Chandra, C., Kim, J., 2021. Controlling intercalation sites of hard carbon for enhancing Na and K storage performance. Chem. Eng. J. 411.
Alvira, D., Antorán, D., Vidal, M., Sebastian, V., Manyà, J.J., 2023. Vine Shoots-Derived Hard Carbons as Anodes for Sodium-Ion. Batter. Role Annealing Temp. Regul. Their Struct. Morphol. Batter. & Supercaps 6.
Au, H., Alptekin, H., Jensen, A.C.S., Olsson, E., O'Keefe, C.A., Smith, T., Crespo-Ribadeneyra, M., Headen, T.F., Grey, C.P., Cai, Q., Drew, A.J., Titirici, M.-M., 2020. A revised mechanistic model for sodium insertion in hard carbons. Energy & Environ. Sci. 13, 3469–3479.
Bai, P., He, Y., Zou, X., Zhao, X., Xiong, P., Xu, Y., 2018. Elucidation of the Sodium-Storage Mechanism in Hard Carbons. Adv. Energy Mater. 8.
Ban, L.L., Crawford, D., Marsh, H., 1975. Lattice-resolution electron microscopy in structural studies of non-graphitizing carbons from polyvinylidene chloride (PVDC). J. Appl. Crystallogr. 8, 415–420.
Beda, A., Taberna, P.-L., Simon, P., Matei Ghimbeu, C., 2018. Hard carbons derived from green phenolic resins for Na-ion batteries. Carbon 139, 248–257.

Beda, A., Rabuel, F., Morcrette, M., Knopf, S., Taberna, P.-L., Simon, P., Matei Ghimbeu, C., 2021. Hard carbon key properties allow for the achievement of high Coulombic efficiency and high volumetric capacity in Na-ion batteries. J. Mater. Chem. A 9, 1743–1758.
Bommier, C., Surta, T.W., Dolgos, M., Ji, X., 2015. New Mechanistic Insights on Na-Ion Storage in Nongraphitizable Carbon. Nano Lett. 15, 5888–5892.
Cao, Y., Xiao, L., Sushko, M.L., Wang, W., Schwenzer, B., Xiao, J., Nie, Z., Saraf, L.V., Yang, Z., Liu, J., 2012. Sodium ion insertion in hollow carbon nanowires for battery applications. Nano Lett. 12, 3783–3787.
Chen, C., Wang, Z., Zhang, B., Miao, L., Cai, J., Peng, L., Huang, Y., Jiang, J., Huang, Y., Zhang, L., Xie, J., 2017. Nitrogen-rich hard carbon as a highly durable anode for high-power potassium-ion batteries. Energy Storage Mater. 8, 161–168.
Chen, W., Wan, M., Liu, Q., Xiong, X., Yu, F., Huang, Y., 2018. Heteroatom-Doped Carbon Materials: Synthesis, Mechanism, and Application for Sodium-Ion Batteries. Small Methods 3.
Chen, W., Gong, M., Li, K., Xia, M., Chen, Z., Xiao, H., Fang, Y., Chen, Y., Yang, H., Chen, H., 2020. Insight into KOH activation mechanism during biomass pyrolysis: Chemical reactions between O-containing groups and KOH. Appl. Energy 278.
Chen, X., Tian, J., Li, P., Fang, Y., Fang, Y., Liang, X., Feng, J., Dong, J., Ai, X., Yang, H., Cao, Y., 2022. An Overall Understanding of Sodium Storage Behaviors in Hard Carbons by an "Adsorption-Intercalation/Filling" Hybrid Mechanism. Adv. Energy Mater. 12.
Chen, Y., Sun, H., He, X.X., Chen, Q., Zhao, J.H., Wei, Y., Wu, X., Zhang, Z., Jiang, Y., Chou, S.L., 2024. Pre-Oxidation Strategy Transforming Waste Foam to Hard Carbon Anodes for Boosting Sodium Storage Performance. Small 20, e2307132.
Chen, Y., Wang, B., Wang, L., Li, J., Deng, H., Zhang, C., Sun, L., Kong, X., Wan, Z., Ou, C., 2026. Preparation of amylase-modified bamboo-based hard carbon for high-performance sodium-ion batteries and study of sodium storage mechanism. J. Energy Storage 149.
Cui, J., Su, P., Li, W., Wang, X., Zhang, Y., Xiao, Z., An, Q., Chen, Z., 2025a. Advanced Cellulose-Derived Hard Carbon as Anode for Sodium-Ion Batteries: Mechanisms, Optimization, and Challenges. Adv. Energy Mater. 15.
Cui, Z., Li, B.-y, Xiong, H., Li, T., Xie, M.-x, Hu, J.-y, Qiu, X., Gui, Z.-q, Zhou, R., Shi, L.-l, Ju, Z.-c, Chen, Y.-x, 2025b. A review of ways to improve the performance of hard carbon anodes in low-temperature sodium-ion batteries. N. Carbon Mater. 40, 1246–1263.
Dahbi, M., Kiso, M., Kubota, K., Horiba, T., Chafik, T., Hida, K., Matsuyama, T., Komaba, S., 2017. Synthesis of hard carbon from argan shells for Na-ion batteries. J. Mater. Chem. A 5, 9917–9928.
Daher, N., Huo, D., Davoisne, C., Meunier, P., Janot, R., 2020. Impact of Preoxidation Treatments on Performances of Pitch-Based Hard Carbons for Sodium-Ion Batteries. ACS Appl. Energy Mater. 3, 6501–6510.
Dayarathne, N.K., Shi, C., Song, X., Yan, C., Wang, D., Wang, H., Zhong, Y.L., Zhang, Z., 2025. Unlocking the potential of lignin for sodium-ion battery anodes: From biorefining to hard carbon engineering. Energy Storage Mater. 83.
Deng, Y., Dai, P., Fu, W., Che, L., Miao, L., Chen, C., Jiao, L., Jin, T., 2025. Heterostructured Solid Electrolyte Interphase Enables Facilitated Kinetics for Low-Temperature Sodium-Ion Batteries. Adv. Funct. Mater. 35.
Dhawale, D.S., Biswas, S., Kaur, G., Giddey, S., 2023. Challenges and advancement in direct ammonia solid oxide fuel cells: a review. Inorg. Chem. Front. 10, 6176–6192.
Ding, J., Wang, H., Li, Z., Kohandehghan, A., Cui, K., Xu, Z., Zahiri, B., Tan, X., Lotfabad, E.M., Olsen, B.C., Mitlin, D., 2013. Carbon nanosheet frameworks derived from peat moss as high performance sodium ion battery anodes. ACS Nano 7, 11004–11015.
Ding, J., Zhou, H., Zhang, H., Stephenson, T., Li, Z., Karpuzov, D., Mitlin, D., 2017. Exceptional energy and new insight with a sodium–selenium battery based on a carbon nanosheet cathode and a pseudographite anode. Energy & Environ. Sci. 10, 153–165.
Dong, Z., 2025. Ind. Prospects Sodium-Ion.-. Batter. are Promis. ⟨https://paper.people.com.cn/zgnyb/pc/content/202512/15/content_30125316.html⟩ (accessed 13 April 2026).
Dou, X., Hasa, I., Hekmatfar, M., Diemant, T., Behm, R.J., Buchholz, D., Passerini, S., 2017. Pectin, Hemicellulose, or Lignin? Impact of the Biowaste Source on the Performance of Hard Carbons for Sodium-Ion Batteries. ChemSusChem 10, 2668–2676.
Dou, X., Hasa, I., Saurel, D., Vaalma, C., Wu, L., Buchholz, D., Bresser, D., Komaba, S., Passerini, S., 2019. Hard carbons for sodium-ion batteries: Structure, analysis, sustainability, and electrochemistry. Mater. Today 23, 87–104.
Escamilla-Pérez, A.M., Beda, A., Simonin, L., Grapotte, M.-L., Le-Meins, J.M., Matei Ghimbeu, C., 2023. Biopolymer-Based Hard Carbons: Correlations between Properties and Performance as a Na-Ion Battery Anode. ACS Appl. Energy Mater. 6, 7419–7432.
Ferrari, A.C., 2007. Raman spectroscopy of graphene and graphite: Disorder, electron–phonon coupling, doping and nonadiabatic effects. Solid State Commun. 143, 47–57.
Ferrari, A.C., Basko, D.M., 2013. Raman spectroscopy as a versatile tool for studying the properties of graphene. Nat. Nanotechnol. 8, 235–246.
Franklin, R.E., 1951. Crystallite growth in graphitizing and non-graphitizing carbons. In: Proceedings of the Royal Society of London. Series A. Mathematical and Physical Sciences, 209, pp. 196–218.
Fu, Z., Jiang, D., Tang, Z., Tang, Z., Zhou, J., Liu, R., Li, H., Sun, D., Tang, Y., Wang, H., 2025. Revealing the blocking effect of hemicellulose on the formation of closed pores in reed-derived hard carbon for sodium-ion batteries. Chem. Eng. J. 505.
Gan, S., Huang, Y., Hong, N., Zhang, Y., Xiong, B., Zheng, Z., He, Z., Gao, S., Deng, W., Zou, G., Hou, H., Ji, X., 2025. Comprehensive Understanding of Closed Pores in Hard Carbon Anode for High-Energy Sodium-Ion Batteries. Nanomicro Lett. 17, 325.
Gao, Y., 2021. Design of hard carbon anode with low specific surface area and low porosity in sodium ion battery. IOP Conference Series Earth Environmental Science 804.
Harris, P.J.F., Tsang, S.C., 1997. High-resolution electron microscopy studies of non-graphitizing carbons. Philos. Mag. A 76, 667–677.
He, H., Sun, D., Tang, Y., Wang, H., Shao, M., 2019. Understanding and improving the initial Coulombic efficiency of high-capacity anode materials for practical sodium ion batteries. Energy Storage Mater. 23, 233–251.
Hong, K.-l, Qie, L., Zeng, R., Yi, Z.-q, Zhang, W., Wang, D., Yin, W., Wu, C., Fan, Q.-j, Zhang, W.-x, Huang, Y.-h, 2014. Biomass derived hard carbon used as a high performance anode material for sodium ion batteries. J. Mater. Chem. A 2.
Hong, Z., Zhen, Y., Ruan, Y., Kang, M., Zhou, K., Zhang, J.M., Huang, Z., Wei, M., 2018. Rational Design and General Synthesis of S-Doped Hard Carbon with Tunable Doping Sites toward Excellent Na-Ion Storage Performance. Adv. Mater., e1802035
Hu, H.-Y., Xiao, Y., Ling, W., Wu, Y.-B., Wang, P., Tan, S.-J., Xu, Y.-S., Guo, Y.-J., Chen, W.-P., Tang, R.-R., Zeng, X.-X., Yin, Y.-X., Wu, X.-W., 2020. A Stable Biomass-Derived Hard Carbon Anode for High-Performance Sodium-Ion Full Battery. Energy Technol. 9.
Hu, X., Ji, Y., Wu, S., Li, S., Shi, Q., Sun, J., Wan, J., Zhao, Y., 2025. Mass-Transfer Engineered Synthesis of Pitch-Derived Hard Carbons for Enhanced Sodium Storage. Adv. Energy Mater. 16.
Huang, J., Liu, L., Fan, Q., Li, S., Cui, H., Xu, J., 2025. Nitrogen-Doped Hard Carbon Anode from Redwood Biomass for Sodium-Ion Batteries with High Initial Coulombic Efficiency and Enhanced Rate Capability. Small 21, e2505579.
Huang, Z., Huang, J., Zhong, L., Zhang, W., Qiu, X., 2024. Deconstruction Engineering of Lignocellulose Toward High-Plateau-Capacity Hard Carbon Anodes for Sodium-Ion Batteries. Small 20, e2405632.
Igarashi, D., Tanaka, Y., Kubota, K., Tatara, R., Maejima, H., Hosaka, T., Komaba, S., 2023. New Template Synthesis of Anomalously Large Capacity Hard Carbon for Na- and K-Ion Batteries. Adv. Energy Mater. 13.
Ji, Y., Li, S., Yuan, T., Shi, Q., Hu, X., Shao, Q., Feng, W., Zhao, Y., 2025. Enhancing the sodium storage performance of hard carbon by constructing thin carbon coatings via esterification reactions. J. Colloid Interface Sci. 677, 719–728.
Jian, Z., Bommier, C., Luo, L., Li, Z., Wang, W., Wang, C., Greaney, P.A., Ji, X., 2017. Insights on the Mechanism of Na-Ion Storage in Soft Carbon Anode. Chem. Mater. 29, 2314–2320.
Jiang, M., Sun, N., Ali Soomro, R., Xu, B., 2021. The recent progress of pitch-based carbon anodes in sodium-ion batteries. J. Energy Chem. 55, 34–47.
Jiao, J., Yi, C., Qiu, X., Yang, D., Fu, F., Liu, W., 2024. Green biomass: the impact of high-adhesion and well-dispersed binders on the sodium storage performance and interfacial interaction of hard carbon anodes. Green. Chem. 26, 6643–6655.
Jin, Y., Sun, S., Ou, M., Liu, Y., Fan, C., Sun, X., Peng, J., Li, Y., Qiu, Y., Wei, P., Deng, Z., Xu, Y., Han, J., Huang, Y., 2018. High-Performance Hard Carbon Anode: Tunable Local Structures and Sodium Storage Mechanism. ACS Appl. Energy Mater. 1, 2295–2305.
Kamiyama, A., Kubota, K., Nakano, T., Fujimura, S., Shiraishi, S., Tsukada, H., Komaba, S., 2019. High-Capacity Hard Carbon Synthesized from Macroporous Phenolic Resin for Sodium-Ion and Potassium-Ion Battery. ACS Appl. Energy Mater. 3, 135–140.
Kamiyama, A., Kubota, K., Igarashi, D., Youn, Y., Tateyama, Y., Ando, H., Gotoh, K., Komaba, S., 2021. MgO-Template Synthesis of Extremely High Capacity Hard Carbon for Na-Ion Battery. Angew. Chem. Int Ed. Engl. 60, 5114–5120.
Kim, D.-Y., Li, O.L., Kang, J., 2020. Novel synthesis of highly phosphorus-doped carbon as an ultrahigh-rate anode for sodium ion batteries. Carbon 168, 448–457.
Kitsu Iglesias, L., Antonio, E.N., Martinez, T.D., Zhang, L., Zhuo, Z., Weigand, S.J., Guo, J., Toney, M.F., 2023. Revealing the Sodium Storage Mechanisms in Hard Carbon Pores. Adv. Energy Mater. 13.
Komaba, S., Murata, W., Ishikawa, T., Yabuuchi, N., Ozeki, T., Nakayama, T., Ogata, A., Gotoh, K., Fujiwara, K., 2011. Electrochemical Na Insertion and Solid Electrolyte Interphase for Hard-Carbon Electrodes and Application to Na-Ion Batteries. Adv. Funct. Mater. 21, 3859–3867.
Kulova, T.L., Skundin, A.M., 2022. Electrode/Electrolyte Interphases of Sodium-Ion Batteries. Energies 15.
Lan, N., Shen, Y., Li, J., He, H., Zhang, C., 2025. Cell-Shearing Chemistry Directed Closed-Pore Regeneration in Biomass-Derived Hard Carbons for Ultrafast Sodium Storage. Adv. Mater. 37, e2412989.
LeGe, N., Zhang, Y.H., Lai, W.H., He, X.X., Wang, Y.X., Zhao, L.F., Liu, M., Wu, X., Chou, S.L., 2025. Potassium escaping balances the degree of graphitization and pore channel structure in hard carbon to boost plateau sodium storage capacity. Chem. Sci. 16, 1179–1188.
Li, H., Zhao, Z., Ai, L., Yang, K., Zhang, F., Wang, X., Qiu, J., 2024. Insight into the configuration of hard-soft carbon composites for high performance sodium-ion batteries. Electrochim. Acta 499.
Li, M., Chen, Y., Qing, Y., Liu, M., Wu, Y., Li, L., 2025a. A novel cascade utilization of Camellia oleifera shell waste for co-production of xylo-oligosaccharides and high-performance hard carbon: processes and mechanisms. Bioresour. Technol. 437, 133101.
Li, N., Li, H., Huang, H., 2025b. Synergistic Nitrogen-Doping and Defect Engineering in Hard Carbon: Unlocking Ultrahigh Rate Capability and Long-Cycling Stability for Sodium-Ion Battery Anodes. Mater. (Basel) 18.
Li, Y., Xu, S., Wu, X., Yu, J., Wang, Y., Hu, Y.-S., Li, H., Chen, L., Huang, X., 2015. Amorphous monodispersed hard carbon micro-spherules derived from biomass as a high performance negative electrode material for sodium-ion batteries. J. Mater. Chem. A 3, 71–77.

Li, Y., Hu, Y.S., Titirici, M.M., Chen, L., Huang, X., 2016a. Hard Carbon Microtubes Made from Renewable Cotton as High-Performance Anode Material for Sodium-Ion Batteries. Adv. Energy Mater. 6.
Li, Y., Mu, L., Hu, Y.-S., Li, H., Chen, L., Huang, X., 2016b. Pitch-derived amorphous carbon as high performance anode for sodium-ion batteries. Energy Storage Mater. 2, 139–145.
Li, Y., Lu, Y., Meng, Q., Jensen, A.C.S., Zhang, Q., Zhang, Q., Tong, Y., Qi, Y., Gu, L., Titirici, M.M., Hu, Y.S., 2019b. Regulating Pore Structure of Hierarchical Porous Waste Cork-Derived Hard Carbon Anode for Enhanced Na Storage Performance. Adv. Energy Mater. 9.
Li, Y., Lu, Y., Adelhelm, P., Titirici, M.M., Hu, Y.S., 2019a. Intercalation chemistry of graphite: alkali metal ions and beyond. Chem. Soc. Rev. 48, 4655–4687.
Li, Z., Bommier, C., Chong, Z.S., Jian, Z., Surta, T.W., Wang, X., Xing, Z., Neuefeind, J.C., Stickle, W.F., Dolgos, M., Greaney, P.A., Ji, X., 2017. Mechanism of Na-Ion Storage in Hard Carbon Anodes Revealed by Heteroatom Doping. Adv. Energy Mater. 7.
Li, Z., Chen, Y., Jian, Z., Jiang, H., Razink, J.J., Stickle, W.F., Neuefeind, J.C., Ji, X., 2018. Defective Hard Carbon Anode for Na-Ion Batteries. Chem. Mater. 30, 4536–4542.
Liang, J., Fan, K., Wei, Z., Gao, X., Song, W., Ma, J., 2018. Porous NaTi2(PO4)3@C nanocubes as improved anode for sodium-ion batteries. Mater. Res. Bull. 99, 343–348.
Liang, P., Huo, Z., Liu, Y., Bo, Z., Wu, Y., Hu, X., Wen, Z., 2025. Biomass-Derived Phosphorus-Doped Porous Hard Carbon Anode for Stable and High-Rate Sodium Ion Batteries. Batter. & Supercaps 8.
Liu, F., 2025. Breakthr. Achieved Negat. Electrode Transp. Kinet. Bottle Sodium-Ion.-. Batter. Nov. Hard Carbon Anode Enables Ultra-Long. Cycle Life 100000 Cycles. ⟨https://portal.las.ac.cn/choiceness/getChoicenessDetail.htm?serverId=207&uuid=4a90af46c5df154e1dcdd39e8e481127&recommendId=164250&controlType=&directionId⟩ (accessed 13 April 2026).
Liu, H., Jia, M., Wang, M., Chen, R., Sun, N., Zhu, Q., Wu, F., Xu, B., 2016. A floral variant of mesoporous carbon as an anode material for high performance sodium and lithium ion batteries. RSC Adv. 6, 78235–78240.
Liu, H., Xu, Z., Guo, Z., Feng, J., Li, H., Qiu, T., Titirici, M., 2021b. A life cycle assessment of hard carbon anodes for sodium-ion batteries. Philos. Trans. A Math. Phys. Eng. Sci. 379, 20200340.
Liu, H., Cheng, C., Wu, H., 2021a. Sustainable utilization of wetland biomass for activated carbon production: A review on recent advances in modification and activation methods. Sci. Total Environ. 790, 148214.
Liu, H., Baumann, M., Moon, H., Zhang, X., Dou, X., Zarrabeitia, M., Crenna, E., Hischier, R., Passerini, S., Assen, N., v.d., Weil, M., 2024. Life cycle assessment of bio-based hard carbon for sodium-ion batteries across different production scales. Chem. Eng. J. 495.
Liu, J., Wen, Y., van Aken, P.A., Maier, J., Yu, Y., 2014. Facile synthesis of highly porous Ni-Sn intermetallic microcages with excellent electrochemical performance for lithium and sodium storage. Nano Lett. 14, 6387–6392.
Liu, J., Li, S., Zhu, J., Yang, C., 2025a. Surface structure optimization of hard carbon to improve its initial coulomb efficiency for sodium-ion storage. Diam. Relat. Mater. 156.
Liu, Y., Chen, S., Zhang, C., Li, G., Liu, J., Wang, Y., 2025b. Shredded-Coconut-Derived Sulfur-Doped Hard Carbon via Hydrothermal Processing for High-Performance Sodium Ion Anodes. Nanomater. (Basel) 15.
Lu, B., Lin, C., Xiong, H., Zhang, C., Fang, L., Sun, J., Hu, Z., Wu, Y., Fan, X., Li, G., Fu, J., Deng, D., Wu, Q., 2023a. Hard-Carbon Negative Electrodes from Biomasses for Sodium-Ion Batteries. Molecules 28.
Lu, H., Chen, X., Jia, Y., Chen, H., Wang, Y., Ai, X., Yang, H., Cao, Y., 2019. Engineering Al2O3 atomic layer deposition: Enhanced hard carbon-electrolyte interface towards practical sodium ion batteries. Nano Energy 64.
Lu, Y., Zhao, C., Qi, X., Qi, Y., Li, H., Huang, X., Chen, L., Hu, Y.S., 2018. Pre-Oxidation-Tuned Microstructures of Carbon Anodes Derived from Pitch for Enhancing Na Storage Performance. Adv. Energy Mater. 8.
Lu, Z., Geng, C., Yang, H., He, P., Wu, S., Yang, Q.H., Zhou, H., 2022. Step-by-step desolvation enables high-rate and ultra-stable sodium storage in hard carbon anodes. Proc. Natl. Acad. Sci. USA 119, e2210203119.
Lu, Z., Wang, J., Feng, W., Yin, X., Feng, X., Zhao, S., Li, C., Wang, R., Huang, Q.A., Zhao, Y., 2023b. Zinc Single-Atom-Regulated Hard Carbons for High-Rate and Low-Temperature Sodium-Ion Batteries. Adv. Mater. 35, e2211461.
Lu, Z., Yang, H., Guo, Y., Lin, H., Shan, P., Wu, S., He, P., Yang, Y., Yang, Q.H., Zhou, H., 2024. Consummating ion desolvation in hard carbon anodes for reversible sodium storage. Nat. Commun. 15, 3497.
Luo, P., Zheng, C., He, J., Tu, X., Sun, W., Pan, H., Zhou, Y., Rui, X., Zhang, B., Huang, K., 2021. Structural Engineering in Graphite-Based Metal-Ion Batteries. Adv. Funct. Mater. 32.
Maka, A.O.M., Chaudhary, T.N., 2024. Performance investigation of solar photovoltaic systems integrated with battery energy storage. J. Energy Storage 84.
Matei Ghimbeu, C., Zhang, B., Martinez de Yuso, A., Réty, B., Tarascon, J.-M., 2019. Valorizing low cost and renewable lignin as hard carbon for Na-ion batteries: Impact of lignin grade. Carbon 153, 634–647.
Materials, B.N., 2023. Bateray Releases First Innov. Achiev. Sodium-Ion.-. Battery Fuel Cell Mater. ⟨https://h2.in-en.com/html/h2-2425197.shtml⟩ (accessed 18 March 2026).
Morikawa, Y., Nishimura, Si, Hashimoto, Ri, Ohnuma, M., Yamada, A., 2019. Mechanism of Sodium Storage in Hard Carbon: An X-Ray Scattering Analysis. Advanced Energy. Materials 10.
Muruganantham, R., Hsieh, T.-H., Lin, C.-H., Liu, W.-R., 2019. Bio-oil derived hierarchical porous hard carbon from rubber wood sawdust via a template fabrication process as highly stable anode for sodium-ion batteries. Mater. Today Energy 14.
Ni, D., Sun, W., Wang, Z., Bai, Y., Lei, H., Lai, X., Sun, K., 2019. Heteroatom-Doped Mesoporous Hollow Carbon Spheres for Fast Sodium Storage with an Ultralong Cycle Life. Adv. Energy Mater. 9.
Palomares, V., Serras, P., Villaluenga, I., Hueso, K.B., Carretero-González, J., Rojo, T., 2012. Na-ion batteries, recent advances and present challenges to become low cost energy storage systems. Energy & Environ. Sci. 5.
Patel, A., Mishra, R., Tiwari, R.K., Tiwari, A., Samriddhi, Singh, S.P., Yadav, V., Singh, R. K., 2024. Nitrogen-Doped Bioderived Mesoporous Hard Carbon as a Promising Anode for Long-Life Sodium-Ion Battery. Energy & Fuels 38, 11262–11274.
Pei, B., Yu, H., Zhang, L., Fang, G., Zhou, J., Cao, X., Liang, S., 2025. Hard Carbon for Sodium-Ion Batteries: From Fundamental Research to Practical Applications. Adv. Mater. 37, e2504574.
Pei, Z., Meng, Q., Wei, L., Fan, J., Chen, Y., Zhi, C., 2020. Toward efficient and high rate sodium-ion storage: A new insight from dopant-defect interplay in textured carbon anode materials. Energy Storage Mater. 28, 55–63.
Peters, J., Buchholz, D., Passerini, S., Weil, M., 2016. Life cycle assessment of sodium-ion batteries. Energy & Environ. Sci. 9, 1744–1751.
Qian, J., Chen, Y., Wu, L., Cao, Y., Ai, X., Yang, H., 2012. High capacity Na-storage and superior cyclability of nanocomposite Sb/C anode for Na-ion batteries. Chem. Commun. (Camb.) 48, 7070–7072.
Qiu, C., Li, A., Qiu, D., Wu, Y., Jiang, Z., Zhang, J., Xiao, J., Yuan, R., Jiang, Z., Liu, X., Chen, X., Song, H., 2024. One-Step Construction of Closed Pores Enabling High Plateau Capacity Hard Carbon Anodes for Sodium-Ion Batteries: Closed-Pore Formation and Energy Storage Mechanisms. ACS Nano 18, 11941–11954.
Raj, H., Franco, A., 2025. Understanding the Manufacturing Processability of Hard Carbon Electrodes to Optimize the Electrochemical Performance of Na-Ion Battery Cells. ECS Meet. Abstr. MA2025-02, 757-757.
Ren, Q., Yang, J., Zhang, P., He, L., Sun, Z., Hao, R., Shi, Z., 2025. Engineering Pore Architecture in Hard Carbon for High-Performance Sodium-Ion Batteries: Distinguishing the Contributions of Ultramicropores and Closed Pores. Adv. Funct. Mater.
Saikia, D., Deka, J.R., Lu, B.-J., Chen, Y.-C., Lian, J.-W., Kao, H.-M., Yang, Y.-C., 2023. Pinecone-derived biomass carbons as anodes for lithium and sodium-ion batteries by template-assisted and chemically activated approaches. J. Power Sources 580.
Saurel, D., Orayech, B., Xiao, B., Carriazo, D., Li, X., Rojo, T., 2018. From Charge Storage Mechanism to Performance: A Roadmap toward High Specific Energy Sodium-Ion Batteries through Carbon Anode Optimization. Adv. Energy Mater. 8.
SECURITIES, S., 2022. Shengquan Group. Leverag-.-. Biomass-.-. Refin. Technol. Dev. Hard Carbon Anode Proj. ⟨https://stock.stockstar.com/JC2022122100003161.shtml⟩ (accessed 18 March 2026).
Shi, G., Han, Z., Hu, L., Wang, B., Huang, F., 2022. N/O Co-Doped Hard Carbon Derived from Cocklebur Fruit for Sodium-Ion Storage. ChemElectroChem 9.
Stevens, D.A., Dahn, J.R., 2000b. An In Situ Small-Angle X-Ray Scattering Study of Sodium Insertion into a Nanoporous Carbon Anode Material within an Operating Electrochemical Cell. J. Electrochem. Soc. 147.
Stevens, D.A., Dahn, J.R., 2000a. High Capacity Anode Materials for Rechargeable Sodium-Ion Batteries. J. Electrochem. Soc. 147.
Stevens, D.A., Dahn, J.R., 2001. The Mechanisms of Lithium and Sodium Insertion in Carbon Materials. J. Electrochem. Soc. 148.
Su, L., Zhang, C., Tang, W., Fu, Z., Gong, J., Qin, J., Li, L., Xia, L., Xu, W., 2024. Moist-electric generators using biomass Juncus effusus fibers with 3D microchannels for wearable applications. Chem. Eng. J. 499.
Sun, D., Zhao, L., Yang, Y., Lu, C., Xu, C., Xiao, Z., Ma, X., 2025a. Thiophene-S doping assisted constructing high-performance pitch-based hard carbon anode for sodium-ion batteries. Mater. Rep. Energy 5.
Sun, F., Wang, H., Qu, Z., Wang, K., Wang, L., Gao, J., Gao, J., Liu, S., Lu, Y., 2020. Carboxyl-Dominant Oxygen Rich Carbon for Improved Sodium Ion Storage: Synergistic Enhancement of Adsorption and Intercalation Mechanisms. Adv. Energy Mater. 11.
Sun, L., Li, J., Li, E., Wang, L., 2025b. Bridging sodium storage behavior and microstructure in broad-leaf lignin hard carbon for sodium-ion batteries. Carbon 233.
Sun, N., Guan, Z., Liu, Y., Cao, Y., Zhu, Q., Liu, H., Wang, Z., Zhang, P., Xu, B., 2019. Extended "Adsorption–Insertion" Model: A New Insight into the Sodium Storage Mechanism of Hard Carbons. Adv. Energy Mater. 9.
Sun, N., Qiu, J., Xu, B., 2022. Understanding of Sodium Storage Mechanism in Hard Carbons: Ongoing Development under Debate. Adv. Energy Mater. 12.
Sun, Z., Li, Z., Li, Y., Wang, Z., Zuo, H., Zhao, L., Liu, X., 2025c. Unveiling a two-stage closed-pore formation mechanism in bamboo-derived hard carbons for high-plateau-capacity sodium-ion battery anodes. Chem. Eng. J. 521.
Terzyk, A.P., Furmaniak, S., Harris, P.J., Gauden, P.A., Wloch, J., Kowalczyk, P., Rychlicki, G., 2007. How realistic is the pore size distribution calculated from adsorption isotherms if activated carbon is composed of fullerene-like fragments? Phys. Chem. Chem. Phys. 9, 5919–5927.
Thompson, M., Xia, Q., Hu, Z., Zhao, X.S., 2021. A review on biomass-derived hard carbon materials for sodium-ion batteries. Mater. Adv. 2, 5881–5905.
de Tomas, C., Alabidun, S., Chater, L., Darby, M.T., Raffone, F., Restuccia, P., Au, H., Titirici, M.M., Cucinotta, C.S., Crespo-Ribadenyra, M., 2023. Doping carbon electrodes with sulfur achieves reversible sodium ion storage. J. Phys. Energy 5.
Townsend, S.J., Lenosky, T.J., Muller, D.A., Nichols, C.S., Elser, V.V., 1992. Negatively curved graphitic sheet model of amorphous carbon. Phys. Rev. Lett. 69, 921–924.
Tsai, P.-c, Chung, S.-C., Lin, S.-k, Yamada, A., 2015. Ab initio study of sodium intercalation into disordered carbon. J. Mater. Chem. A 3, 9763–9768.

Vasileiadis, A., Li, Y., Lu, Y., Hu, Y.S., Wagemaker, M., 2023. Role of Defects, Pores, and Interfaces in Deciphering the Alkali Metal Storage Mechanism in Hard Carbon. ACS Appl. Energy Mater. 6, 127–140.
Wang, C.-C., Su, W.-L., 2021. Ultrathin Artificial Solid Electrolyte Interface Layer-Coated Biomass-Derived Hard Carbon as an Anode for Sodium-Ion Batteries. ACS Appl. Energy Mater. 5, 1052–1064.
Wang, J., Yan, L., Ren, Q., Fan, L., Zhang, F., Shi, Z., 2018a. Facile hydrothermal treatment route of reed straw-derived hard carbon for high performance sodium ion battery. Electrochim. Acta 291, 188–196.
Wang, J., Huang, Z., Zhang, W., Li, Q., Liang, Z., Lu, J., Lin, Z., Wang, G., Wu, J., Huang, S., 2024a. Balancing Graphitic Nanodomains and Heteroatom Doping in Hard Carbons Toward High Capacity and Durable Potassium-Ion Battery Anodes. Adv. Funct. Mater. 34.
Wang, J., Fan, J., Yue, X., Fan, M., Xie, Z., Yang, Z., Zhang, J., Abudula, A., Guan, G., 2025a. Hard carbon anodes for advanced sodium ion batteries: A review on sodium storage mechanism and strategies to improve the initial Coulombic efficiency. Chem. Eng. J. 511.
Wang, M., Wang, Q., Ding, X., Wang, Y., Xin, Y., Singh, P., Wu, F., Gao, H., 2022. The prospect and challenges of sodium-ion batteries for low-temperature conditions. Interdiscip. Mater. 1, 373–395.
Wang, Y., Xiao, N., Wang, Z., Tang, Y., Li, H., Yu, M., Liu, C., Zhou, Y., Qiu, J., 2018b. Ultrastable and high-capacity carbon nanofiber anodes derived from pitch/polyacrylonitrile for flexible sodium-ion batteries. Carbon 135, 187–194.
Wang, Y., Yi, Z., Xie, L., Mao, Y., Ji, W., Liu, Z., Wei, X., Su, F., Chen, C.M., 2024b. Releasing Free Radicals in Precursor Triggers the Formation of Closed Pores in Hard Carbon for Sodium-Ion Batteries. Adv. Mater. 36, e2401249.
Wang, Y., Yu, Z., Li, Q., Liu, Y., 2025b. Recent advances in presodiation strategies for hard carbon anodes in sodium-ion batteries. Chem. Commun. (Camb.) 61, 15061–15067.
Wenzel, S., Hara, T., Janek, J., Adelhelm, P., 2011. Room-temperature sodium-ion batteries: Improving the rate capability of carbon anode materials by templating strategies. Energy & Environ. Sci. 4.
Wu, C., Yang, Y., Zhang, Y., Xu, H., Huang, W., He, X., Chen, Q., Dong, H., Li, L., Wu, X., Chou, S., 2024a. Industrial-Scale Hard Carbon Designed to Regulate Electrochemical Polarization for Fast Sodium Storage. Angew. Chem. Int Ed. Engl. 63, e202406889.
Wu, F., Dong, R., Bai, Y., Li, Y., Chen, G., Wang, Z., Wu, C., 2018a. Phosphorus-Doped Hard Carbon Nanofibers Prepared by Electrospinning as an Anode in Sodium-Ion Batteries. ACS Appl. Mater. Interfaces 10, 21335–21342.
Wu, J.B., Lin, M.L., Cong, X., Liu, H.N., Tan, P.H., 2018b. Raman spectroscopy of graphene-based materials and its applications in related devices. Chem. Soc. Rev. 47, 1822–1873.
Wu, S., Lu, X., Zhang, K., Xu, J., Sun, Z., 2022a. Nitrogen/Phosphorus Dual-Doped Hard Carbon Anode with High Initial Coulombic Efficiency for Superior Sodium Storage. Batter. & Supercaps 6.
Wu, S., Peng, H., Xu, J., Huang, L., Liu, Y., Xu, X., Wu, Y., Sun, Z., 2024b. Nitrogen/phosphorus co-doped ultramicropores hard carbon spheres for rapid sodium storage. Carbon 218.
Wu, X.-S., Dong, X.-L., Wang, B.-Y., Xia, J.-L., Li, W.-C., 2022b. Revealing the sodium storage behavior of biomass-derived hard carbon by using pure lignin and cellulose as model precursors. Renew. Energy 189, 630–638.
Xiao, B., Rojo, T., Li, X., 2019. Hard Carbon as Sodium-Ion Battery Anodes: Progress and Challenges. ChemSusChem 12, 133–144.
Xiao, L., Lu, H., Fang, Y., Sushko, M.L., Cao, Y., Ai, X., Yang, H., Liu, J., 2018. Low-Defect and Low-Porosity Hard Carbon with High Coulombic Efficiency and High Capacity for Practical Sodium Ion Battery Anode. Adv. Energy Mater. 8.
Xie, F., Xu, Z., Jensen, A.C.S., Au, H., Lu, Y., Araullo-Peters, V., Drew, A.J., Hu, Y.S., Titirici, M.M., 2019a. Hard–Soft Carbon Composite Anodes with Synergistic Sodium Storage Performance. Adv. Funct. Mater. 29.
Xie, F., Xu, Z., Jensen, A.C.S., Ding, F., Au, H., Feng, J., Luo, H., Qiao, M., Guo, Z., Lu, Y., Drew, A.J., Hu, Y.-S., Titirici, M.-M., 2019b. Unveiling the role of hydrothermal carbon dots as anodes in sodium-ion batteries with ultrahigh initial coulombic efficiency. J. Mater. Chem. A 7, 27567–27575.
Xie, L., Tang, C., Bi, Z., Song, M., Fan, Y., Yan, C., Li, X., Su, F., Zhang, Q., Chen, C., 2021. Hard Carbon Anodes for Next-Generation Li-Ion Batteries: Review and Perspective. Adv. Energy Mater. 11.
Xu, R., Liu, Q., Yang, Q., Yang, W., Mu, D., Li, C., Li, L., Chen, R., Wu, F., 2023a. Study on carbonate ester and ether-based electrolytes and hard carbon anodes interfaces for sodium-ion batteries. Electrochim. Acta 462.
Xu, T., Qiu, X., Zhang, X., Xia, Y., 2023b. Regulation of surface oxygen functional groups and pore structure of bamboo-derived hard carbon for enhanced sodium storage performance. Chem. Eng. J. 452.
Xue, Y., Chen, Y., Liang, Y., Shi, L., Ma, R., Qiu, X., Li, Y., Guo, N., Zhuang, Q., Xi, B., Ju, Z., Xiong, S., 2025. Substitution Index-Prediction Rules for Low-Potential Plateau of Hard Carbon Anodes in Sodium-Ion Batteries. Adv. Mater. 37, e2417886.
Yabuuchi, N., Kubota, K., Dahbi, M., Komaba, S., 2014. Research development on sodium-ion batteries. Chem. Rev. 114, 11636–11682.
Yan, J., Li, W., Feng, P., Wang, R., Jiang, M., Han, J., Cao, S., Wang, K., Jiang, K., 2020. Enhanced Na+ pseudocapacitance in a P, S co-doped carbon anode arising from the surface modification by sulfur and phosphorus with C–S–P coupling. J. Mater. Chem. A 8, 422–432.
Yan, J., Li, H., Wang, K., Jin, Q., Lai, C., Wang, R., Cao, S., Han, J., Zhang, Z., Su, J., Jiang, K., 2021. Ultrahigh Phosphorus Doping of Carbon for High-Rate Sodium Ion Batteries Anode. Adv. Energy Mater. 11.
Yang, B., Wang, J., Zhu, Y., Ji, K., Wang, C., Ruan, D., Xia, Y., 2021a. Engineering hard carbon with high initial coulomb efficiency for practical sodium-ion batteries. J. Power Sources 492.
Yang, G., Li, X., Guan, Z., Tong, Y., Xu, B., Wang, X., Wang, Z., Chen, L., 2020. Insights into Lithium and Sodium Storage in Porous Carbon. Nano Lett. 20, 3836–3843.
Yang, J., Wang, X., Dai, W., Lian, X., Cui, X., Zhang, W., Zhang, K., Lin, M., Zou, R., Loh, K.P., Yang, Q.H., Chen, W., 2021b. From Micropores to Ultra-micropores inside Hard Carbon: Toward Enhanced Capacity in Room-/Low-Temperature Sodium-Ion Storage. Nanomicro Lett. 13, 98.
Yanilmaz, M., Temel, B., Bayram, E., Tosun, M., Topcu, I., Kim, J., 2025. Sustainable biowaste conversion into microporous carbons for efficient energy storage solutions in sodium-ion batteries. J. Environ. Chem. Eng. 13.
Yin, X., Wang, Z., Liu, Y., Lu, Z., Long, H., Liu, T., Zhang, J., Zhao, Y., 2023. Insight into the influence of ether and ester electrolytes on the sodium-ion transportation kinetics for hard carbon. Nano Res. 16, 10922–10930.
You, S., Zhang, Q., Liu, J., Deng, Q., Sun, Z., Cao, D., Liu, T., Amine, K., Yang, C., 2024. Hard carbon with an opened pore structure for enhanced sodium storage performance. Energy & Environ. Sci. 17, 8189–8197.
Youn, Y., Gao, B., Kamiyama, A., Kubota, K., Komaba, S., Tateyama, Y., 2021. Nanometer-size Na cluster formation in micropore of hard carbon as origin of higher-capacity Na-ion battery. npj Comput. Mater. 7.
Yu, C., Li, Y., Ren, H., Qian, J., Wang, S., Feng, X., Liu, M., Bai, Y., Wu, C., 2022a. Engineering homotype heterojunctions in hard carbon to induce stable solid electrolyte interfaces for sodium-ion batteries. Carbon Energy 5.
Yu, C.X., Li, Y., Wang, Z.H., Wang, X.R., Bai, Y., Wu, C., 2022b. Surface engineering based on in situ electro-polymerization to boost the initial Coulombic efficiency of hard carbon anode for sodium-ion battery. Rare Met. 41, 1616–1625.
Yu, S., Sun, N., Hu, L., Wang, L., Zhu, Q., Guan, Y., Xu, B., 2018. Self-template and self-activation synthesis of nitrogen-doped hierarchical porous carbon for supercapacitors. J. Power Sources 405, 132–141.
Yu, Z., Li, X., Sun, N., Chen, H., Soomro, R.A., Xu, B., 2025. Synergistic regulation of closed pore architecture and interface engineering in hard carbon for high energy density sodium-ion batteries. Energy Storage Mater. 82.
Yuan, L., Zhang, Q., Pu, Y., Qiu, X., Liu, C., Wu, H., 2024a. Modulating Intrinsic Defect Structure of Fibrous Hard Carbon for Super-Fast and High-Areal Sodium Energy Storage. Adv. Energy Mater. 14.
Yuan, M., Yu, S., Wang, K., Mi, C., Shen, L., 2024b. Ultrafast synthesis of hard carbon for high-rate and low-temperature sodium-ion storage through flash Joule heating. Solid State Ion. 414.
Yuan, W., Li, X., Lu, X., Wu, M., Liu, J., Zhang, Q., Sun, Z., 2025. Pre-sodiation strategies for sodium-ion batteries with hard carbon anodes: Techniques, challenges, and future directions. Materials Science Engineering B 319.
Zhang, B., Ghimbeu, C.M., Laberty, C., Vix-Guterl, C., Tarascon, J.M., 2015. Correlation Between Microstructure and Na Storage Behavior in Hard Carbon. Adv. Energy Mater. 6.
Zhang, D., Zhang, H., Gao, F., Huang, G., Shang, Z., Gao, C., Chen, X., Wei, J., Terrones, M., Wang, Y., 2024a. Dual Activation for Tuning N, S Co-Doping in Porous Carbon Sheets Toward Superior Sodium Ion Storage. Small 20, e2308684.
Zhang, F., Qin, D., Xu, J., Liu, Z., Zhao, Y., Zhang, X., 2019. Nitrogen and oxygen co-doping carbon microspheres by a sustainable route for fast sodium-ion batteries. Electrochim. Acta 303, 140–147.
Zhang, G., Zhang, L., Ren, Q., Yan, L., Zhang, F., Lv, W., Shi, Z., 2021a. Tailoring a Phenolic Resin Precursor by Facile Pre-oxidation Tactics to Realize a High-Initial-Coulombic-Efficiency Hard Carbon Anode for Sodium-Ion Batteries. ACS Appl. Mater. Interfaces 13, 31650–31659.
Zhang, H., Ming, H., Zhang, W., Cao, G., Yang, Y., 2017. Coupled Carbonization Strategy toward Advanced Hard Carbon for High-Energy Sodium-Ion Battery. ACS Appl. Mater. Interfaces 9, 23766–23774.
Zhang, H., Luo, C., He, H., Wu, H.H., Zhang, L., Zhang, Q., Wang, H., Wang, M.S., 2020. Nano-size porous carbon spheres as a high-capacity anode with high initial coulombic efficiency for potassium-ion batteries. Nanoscale Horiz. 5, 895–903.
Zhang, H., Huang, Z., Lin, S., Cui, J., Zhang, Q., Luo, X., Wang, R., Zhang, C., Shu, C., Tang, W., 2025a. Rational phosphating layer design in biomass-derived hard carbons toward fast charging capability of sodium ion battery anodes. Chem. Sci. 16, 16678–16689.
Zhang, H., Lin, S., Shu, C., Tang, Z., Wang, X., Wu, Y., Tang, W., 2025b. Advances and perspectives of hard carbon anode modulated by defect/hetero elemental engineering for sodium ion batteries. Mater. Today 85, 231–252.
Zhang, J., Huang, Y., Chen, C., She, K., 2023. Boron–Phosphorus Codoped Coral-like Hard Carbon Anodes for Sodium Ion Storage. Energy & Fuels 37, 2379–2386.
Zhang, R., Wang, Y., Zhou, H., Lang, J., Xu, J., Xiang, Y., Ding, S., 2018. Mesoporous TiO (2) nanosheets anchored on graphene for ultra long life Na-ion batteries. Nanotechnology 29, 225401.
Zhang, T., Zhang, T., Wang, F., Ran, F., 2024b. High-efficiently doping nitrogen in kapok fiber-derived hard carbon used as anode materials for boosting rate performance of sodium-ion batteries. J. Energy Chem. 96, 472–482.
Zhang, T., Zhang, T., Wang, F., Zhang, L., Kong, H., Li, Y., Ran, F., 2025c. Heterogeneous Carbon Designed with Disorder-in-Ordered Nanostructure toward High-Rate and Ultra-stable Sodium Ion Storage. Small 21, e2407861.
Zhang, W., Lu, J., Guo, Z., 2021b. Challenges and future perspectives on sodium and potassium ion batteries for grid-scale energy storage. Mater. Today 50, 400–417.
Zhang, X., Cao, Y., Li, G., Liu, G., Dong, X., Wang, Y., Jiang, X., Zhang, X., Xia, Y., 2024c. Exploring Carbonization Temperature to Create Closed Pores for Hard Carbon as High-Performance Sodium-Ion Battery Anodes. Small 20, e2311197.
Zhao, D., Xie, D., Liu, H., Hu, F., Wu, X., 2018. Flexible α-Fe2O3 nanorod electrode materials for sodium-ion batteries with excellent cycle performance. Funct. Mater. Lett. 11.
Zhao, L.F., Hu, Z., Lai, W.H., Tao, Y., Peng, J., Miao, Z.C., Wang, Y.X., Chou, S.L., Liu, H. K., Dou, S.X., 2020. Hard Carbon Anodes: Fundamental Understanding and

Commercial Perspectives for Na-Ion Batteries beyond Li-Ion and K-Ion Counterparts. Adv. Energy Mater. 11.
Zhao, T., Wang, L., Zhang, C., Liu, N., Ouyang, C., Wang, Z., Chen, L., 2025. Comprehensive insights into sodium storage in pitch-derived porous hard carbon. Carbon Energy 7.
Zhao, W., Guo, C., Li, C.M., 2017. Lychee-like FeS2@FeSe2 core–shell microspheres anode in sodium ion batteries for large capacity and ultralong cycle life. J. Mater. Chem. A 5, 19195–19202.
Zheng, S., Tian, Y., Li, W., Wang, B., 2022. CO(2) Etching Modulates Lithium and Sodium Storage Performance of Hard-Soft Carbon Composite-Based Freestanding Thick Electrodes. ACS Appl. Mater. Interfaces 14, 45526–45532.
Zheng, Y., Lu, Y., Qi, X., Wang, Y., Mu, L., Li, Y., Ma, Q., Li, J., Hu, Y.-S., 2019. Superior electrochemical performance of sodium-ion full-cell using poplar wood derived hard carbon anode. Energy Storage Mater. 18, 269–279.
Zhou, H., Song, Y., Zhang, B., Sun, H., Khurshid, I.A., Kong, Y., Chen, L., Cui, L., Zhang, D., Wang, W., Yang, L., Du, X., 2024. Overview of electrochemical competing process of sodium storage and metal plating in hard carbon anode of sodium ion battery. Energy Storage Mater. 71.
Zhou, R., Peng, S., Wang, Z., Zhao, Y., Bao, C., Xia, Y., Zhu, Y., Yang, H., Bo, Z., Yu, Q., 2025. Dynamic Sodiation-Driven Pore Reconstruction for Superior Initial-Coulombic-Efficiency and High-Rate in Xylose-Based Hard Carbon Anode. Adv. Funct. Mater. 35.
Zhu, Y.-E., Gu, H., Chen, Y.-N., Yang, D., Wei, J., Zhou, Z., 2017. Hard carbon derived from corn straw piths as anode materials for sodium ion batteries. Ionics 24, 1075–1081.
Zlatev, D., 2024. Wood-Based Sodium-Ion.-. Battery Electrodes Form. Found. Most Sustain. Batter. Free Lithium Cobalt. ⟨https://www.notebookcheck-cn.com/847181.0.html⟩ (accessed 18 March 2026).